Paleoceanography and Paleoclimatology

RESEARCH ARTICLE
10.1029/2023PA004762

Special Collection:
Illuminating a Warmer World: Insights from the Paleogene

Extreme Planktic Foraminiferal Dwarfism Across the ETM2 in the Tethys Realm in Response to Warming

R. D'Onofrio[1,2], R. Barrett[3], D. N. Schmidt[3], E. Fornaciari[4], L. Giusberti[4], G. Frijia[1], T. Adatte[5], N. Sabatino[6], A. Monsuru[3], V. Brombin[1], and V. Luciani[1]

[1]Dipartimento di Fisica e Scienze della Terra, Università di Ferrara, Ferrara, Italy, [2]Istituto di Scienze Marine (ISMAR), CNR, Venezia, Italy, [3]School of Earth Sciences, University of Bristol, Bristol, UK, [4]Dipartimento di Geoscienze, Università di Padova, Padova, Italy, [5]GEOPOLIS, ISTE, Lausanne University, Lausanne, Switzerland, [6]Istituto per lo studio degli impatti Antropici e Sostenibilità in ambiente marino (IAS), CNR, Palermo, Italy

Abstract Pronounced warming negatively impacts ecosystem resilience in modern oceans. To offer a long-term geological perspective of the calcareous plankton response to global warming, we present an integrated record, from two Tethyan sections (northeastern Italy), of the planktic foraminiferal and calcareous nannofossil response to the Eocene Thermal Maximum 2 hyperthermal (ETM2, ~54 Ma). Our study reveals pronounced changes in assemblage composition and a striking dwarfing of planktic foraminiferal tests of up to 40% during the event, impacting both surface and deeper dwellers. The increased abundance of small placoliths among calcareous nannofossils is interpreted as community size reduction. Literature and our foraminiferal size data from Sites 1263 and 1209 (Atlantic and Pacific Oceans) highlights that the pronounced dwarfism is restricted to the Tethyan area. The ETM2 is characterized by warm sea surface temperatures as indicated by our $\delta^{18}O$ data, but this warming is of global extent and cannot explain the unique dwarfism. Excluding evolutionary modifications, other potential drivers of dwarfism (eutrophication, deoxygenation, metabolic adaptation) cannot explain the exceptional dwarfism by themselves. The smallest sizes are in close temporal association with peaks in volcanic derived Hg/Th-Hg/Rb recorded just before and at the ETM2 which could not have been brought into our sections through weathering. In contrast, size reductions are absent below and above the ETM2 at Hg peaks where $\delta^{18}O$ data do not show warm conditions. We speculate that the local input of toxic metals from submarine volcanic emissions could have acted synergistically to warming, causing the unique dwarfism.

Key Points:

- Calcareous plankton size in the Tethys during the Eocene Thermal Maximum 2 (ETM2) reveals marked dwarfism
- Pronounced dwarfism was restricted to the Tethyan area, highlighting the importance of local signals in interpreting hyperthermals
- Calcareous plankton were highly unstable across the ETM2 but ultimately resilient

Supporting Information:

Supporting Information may be found in the online version of this article.

Correspondence to:

V. Luciani,
valeria.luciani@unife.it

Citation:

D'Onofrio, R., Barrett, R., Schmidt, D. N., Fornaciari, E., Giusberti, L., Frijia, G., et al. (2024). Extreme planktic foraminiferal dwarfism across the ETM2 in the Tethys realm in response to warming. *Paleoceanography and Paleoclimatology*, *39*, e2023PA004762. https://doi.org/10.1029/2023PA004762

Received 15 SEP 2023
Accepted 3 APR 2024

Author Contributions:

Conceptualization: R. D'Onofrio, V. Luciani
Data curation: R. D'Onofrio, R. Barrett, D. N. Schmidt, E. Fornaciari, T. Adatte
Funding acquisition: D. N. Schmidt, L. Giusberti
Investigation: R. D'Onofrio, R. Barrett, D. N. Schmidt, E. Fornaciari, T. Adatte, N. Sabatino, A. Monsuru, V. Luciani

1. Introduction

Climate-induced environmental perturbations are compromising the stability of marine ecosystems. Impacts in the modern ocean range from migration to higher latitudes and deeper waters, reduction in growth, reproduction and other physiological processes, to local extinctions. However, as highlighted in the most recent IPCC (Intergovernmental Panel on Climate Change) report, modern studies are time-limited and do not allow for acclimation or evolutionary adaptation (Pörtner et al., 2022). Therefore, the threat to marine ecosystem health and their services remain uncertain. Combining modern experiments and observation with the huge archive available in the geologic record will increase our understanding by providing constraints for realistic projections of future marine ecosystem impacts.

The early Paleogene climate offers a unique opportunity to evaluate marine ecosystem resilience to environmental perturbations linked to warmth at a multi-millennial time scale perspective, that is, the ability of a population to resist disturbance (e.g., via migration) and/or recover from disturbance (e.g., Capdevila et al., 2020) by returning to a stable state (Hodgson et al., 2015). This time interval is characterized by short-term global warming events, known as hyperthermals (Thomas et al., 2000). Hyperthermals share similar characteristics such as negative excursions in $\delta^{18}O$ and $\delta^{13}C$ records and evidence for dissolution of deep-sea carbonates due to Carbonate Compensation Depth (CCD)/lysocline shallowing, albeit at different magnitudes (e.g., Cramer et al., 2003; Littler et al., 2014; Zachos et al., 2005). Paleogene hyperthermals had a duration between 10^3 and 10^5 Kyr (e.g., Westerhold et al., 2018) were paced by a long (405 Kyr) and short (100 Kyr) eccentricity cycle. Although they are linked to emissions of isotopically depleted CO_2 into the ocean-atmosphere system (e.g., Cramer et al., 2003; Littler et al., 2014; Lourens et al., 2005; Zachos et al., 2010), the source of carbon is debated and may differ between events (e.g., Dickens, 2011; Gutjahr et al., 2017; Kirtland-Turner et al., 2014; Zeebe et al., 2009).

Methodology: R. D'Onofrio, D. N. Schmidt, E. Fornaciari, T. Adatte, V. Luciani
Supervision: D. N. Schmidt, V. Luciani
Writing – original draft: R. D'Onofrio, V. Luciani
Writing – review & editing: R. D'Onofrio, R. Barrett, D. N. Schmidt, E. Fornaciari, L. Giusberti, G. Frijia, T. Adatte, V. Brombin, V. Luciani

In this study, we focus on the impact of the Eocene Thermal Maximum 2 (ETM2) hyperthermal on planktic foraminiferal and calcareous nannofossil assemblages from the Tethyan Terche and Madeago sections (north-eastern Italy) (Figure 1).

The ETM2, referred to as ELMO in Lourens et al. (2005) and H1 in Cramer et al. (2003), occurred at 54.02 Ma, roughly two myrs after the Paleocene Eocene Thermal Maximum (PETM or ETM1, e.g., Westerhold et al., 2018 and references therein). The ETM2 is marked by a ∼1‰ negative Carbon Isotope Excursion (CIE) in marine carbonates and is associated with a ∼3.5°C increase in sea-surface temperature (e.g., Littler et al., 2014; Sluijs et al., 2009; Stap et al., 2009, 2010a, b). In contrast to the pronounced warming of the PETM, the marine biotic record across the ETM2 is less investigated and focusses on individual groups, for example, benthic foraminifera (Jennions et al., 2015), calcareous nannofossils (Dedert et al., 2012; Gibbs et al., 2012) and planktic foraminifera (Davis et al., 2022). These papers do not evaluate the integrated response of calcifying plankton (planktic foraminifera and calcareous nannofossils) to the ETM2 perturbation, or investigate important morphological features such as how their body size changes. Changes in the size of marine calcifiers can indicate evolutionary change or the response to environmental stress, both potential consequences of extreme warmth (e.g., Schmidt et al., 2006 and reference therein).

With the aim to assess the impact of the ETM2 on planktic foraminifera and calcareous nannoplankton and their size, we quantify changes in calcareous plankton assemblages in the Tethys. To provide an environmental context, we analyze geochemical proxies from the two successions. We place our size data into a wider context by comparing it to data from the southern Atlantic Ocean ODP (Ocean Drilling Program) Site 1263 and tropical Pacific ODP Site 1209.

2. Settings, Lithology and Biostratigraphy

The studied Madeago and Terche sections are located in the Venetian Southern Alps of north-eastern Italy (Figure 1) and are part of the Upper Cretaceous-lower Eocene pelagic-hemipelagic succession, deposited in Belluno Basin (e.g., Bosellini, 1989). The Madeago section (46° 6' 20.24"N, 12° 14' 49.54"E) is 8 km southeast of the Belluno town and crops out along the Madeago Valley. We sampled ∼8 m of grayish calcareous marls interrupted at 5 m from the base by a 1.37 m package of gray and reddish clayey marls referred in the local literature to "Marna della Vena d'Oro." Such package of gray and reddish clayey marls (marly unit, MU hereafter) is the lithological expression of the ETM2, as described in D'Onofrio et al. (2016).

The Terche section, previously investigated by D'Onofrio et al. (2016), is located approximately 2 km south of the Mel village (Belluno). It consists of more than 85 m of pink-reddish to green scaly calcareous marls and marly limestones, locally rhythmically organized, referred to as the Scaglia Rossa. We focused on the interval

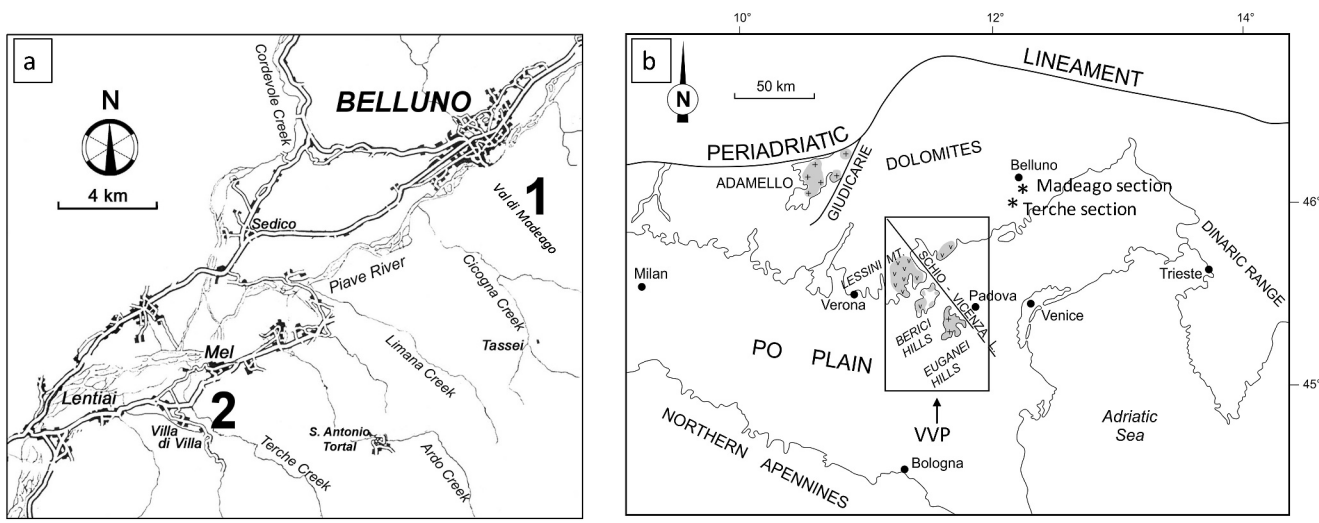

Figure 1. (a) Location map of the studied sections. 1: Madeago, 2: Terche. (b) Schematic map of the Southern Alps, showing the area of the Venetian Volcanic Province (VVP) and the location of the studied sections.

corresponding to the MU that is the lithological expression of the ETM2 event as in Madeago (for more details see D'Onofrio et al., 2016). In D'Onofrio et al. (2016) this interval was labeled as MU 1 because the Terche section records other marly units.

The Plankton-Benthos ratio (P/B) and benthic foraminiferal assemblages at Madeago are analogous to those of the Terche section (D'Onofrio et al., 2016). Across the ETM2 interval at both sections (Figure 4) benthic foraminiferal assemblages are characterized by a great abundance of infaunal calcareous hyaline taxa, especially bolivinids. This is likely linked to a lateral input of refractory organic matter, and is analogous to the PETM in the same area (Giusberti et al., 2016). Taxa indicative of bathyal depth, such as *Cibicidoides eocaenus*, *Aragonia* sp., *Nuttallides truempyi*, *Oridorsalis umbonatus* (Tjalsma & Lohmann, 1983; Van Morkhoven et al., 1986) occur throughout the sections. In addition, the presence of scattered *Abysammina* sp. individuals, which have an upper depth limit of ~ 1.000 m (e.g., Holbourn et al., 2013; Van Morkhoven et al., 1986), argues for a paleodepth close to the middle bathyal/lower bathyal boundary *sensu* Van Morkhoven et al. (1986). The occurrence of abundant cibicidids in the section does not contrast with this interpretation as these forms can live down to abyssal depths (e.g., Murray, 1991).

The Madeago interval studied here spans the planktic foraminiferal Zone E4 (Wade et al., 2011) and calcareous nannofossils Zones CP8 to CP10 of Okada and Bukry (1980) and Zones CN2 to CN3 *pars* of Agnini et al. (2014). The same calcareous plankton zones were detected at the Madeago section as previously identified for the Terche section (D'Onofrio et al., 2016).

3. Methods

Methods for the evaluation of carbonate content, stable isotopes, relative abundances of calcareous plankton, radiolarians and dissolution proxies for the Madeago section (data are reported in Tables S1–S10 in Supporting Information S1 (D'Onofrio et al., 2024)) are the same as applied for Terche. They are described in detail by D'Onofrio et al. (2016). The ETM2 in the cited sites has been identified by the negative shift in $\delta^{13}C$. Stable isotope data from Sites 1209 and 1263 are from Westerhold et al. (2018, 2020), respectively.

3.1. Geochemical Proxies

We carried out analyses of the total organic carbon (TOC), mercury (Hg) and other trace metal concentration from the studied intervals of the Madeago and Terche sections.

At Madeago we analyzed 40 samples spaced at ~2–10 cm across the MU and 20–60 cm below and above, whereas at Terche we analyzed 45 samples from the interval spanning the MU (−7.9 m to +3.0 m). In addition, XRF trace elements data were obtained from 20 (Terche) and 21 (Madeago) samples. These geochemical analyses were performed at Lausanne University.

To characterize environmental background conditions at Terche and Madeago during the ETM2 we evaluated the concentration of trace-element (TE) data obtained by X-ray fluorescence (XRF) focusing on those potentially deriving from volcanic releases (such as Hg, Cr, As, Pb) and on those considered as tracers of detrital influx (clay minerals—phyllosilicates, such as Th and Rb) (Figures 2 and 3, Figures S1, S2, Table S3 in Supporting Information S1). Mercury (Hg) has been described as one of the best tools to detect volcanic activity in the sedimentary record (e.g., Grasby et al., 2019). Nonetheless, Hg has a complex biogeochemical cycle and its signature can be strongly affected by biological or sedimentary processes as well as by local/regional marine conditions (see Supporting Information S1 for a comprehensive discussion on Hg uptake/enrichments in sediments).

The Hg concentration measurements and Rock-Eval Pyrolysis were performed on the same set of whole-rock samples analyzed for carbon and oxygen isotopes. Hg contents were determined at the University of Lausanne (Switzerland) using a Zeeman R-915F (Lumex, St. Petersburg, Russia) high-frequency atomic absorption spectrometer set at Mode 1 (700°C). The samples were analyzed in duplicates, and a certified external standard (Chinese alluvium GSD-11, 72.0 ± 9 ppb Hg; Zintwana et al., 2012) was used for calibration (r = 0.99, for measured vs. certified values) and to guarantee the analytical quality.

An increasing number of studies have shown that Hg geochemistry is complex and can be easily interfered with by local factors, rendering the use of Hg enrichment ineffective in tracing volcanism (Jin et al., 2023; Them et al., 2019). These factors include the transport pathway (Font et al., 2022; Liu et al., 2021), early diagenetic

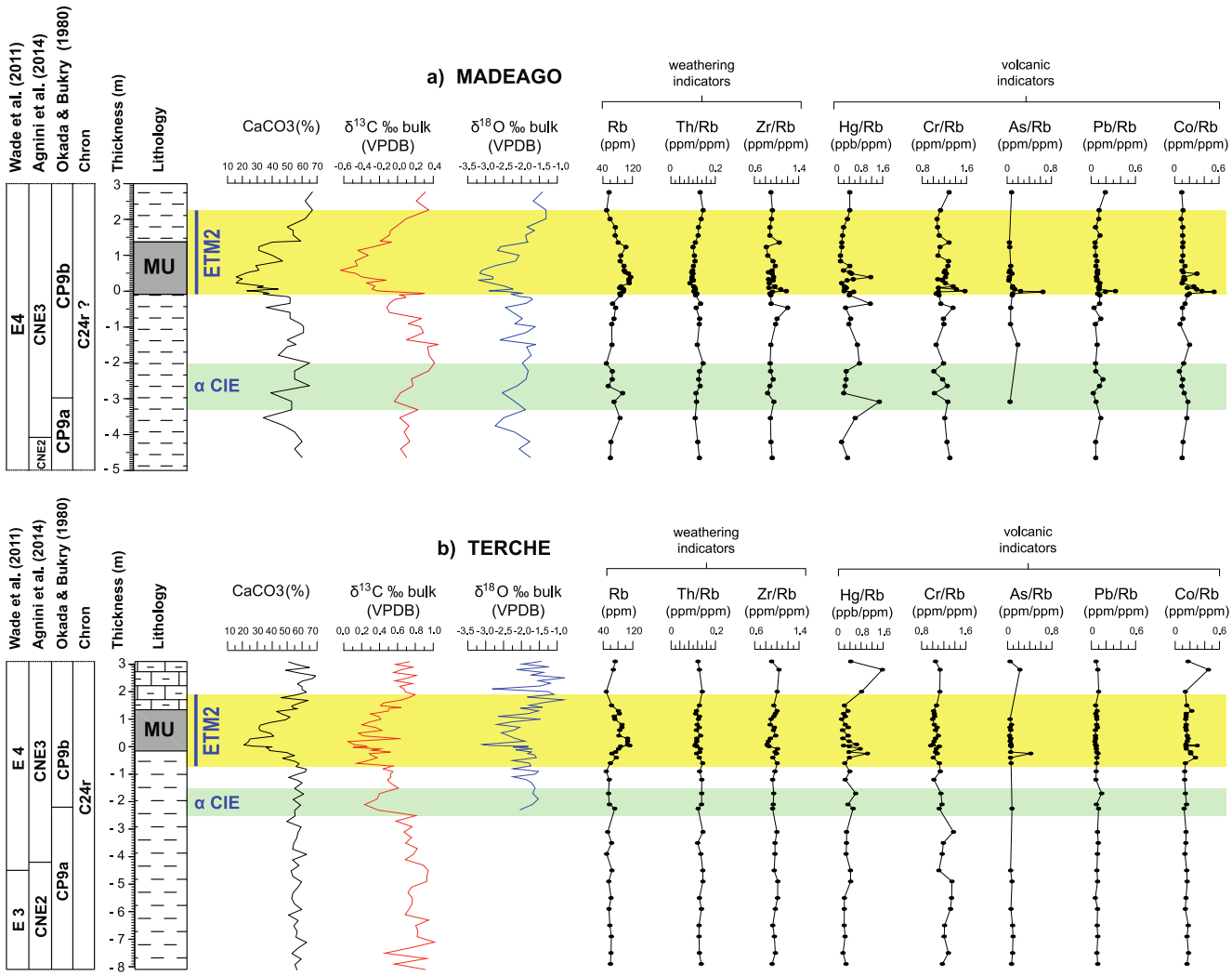

Figure 2. $CaCO_3$ content and geochemical data from the Madeago (a) and Terche (b) sections with stratigraphic logs and biostratigraphy. As in the following figures, the yellow and light-green bands highlight the ETM2 interval as defined by the $\delta^{13}C$ shifts and the α CIE interval respectively.

processes, and excessive TOC levels (Frieling et al., 2023). Charbonnier et al. (2020), evaluating the potential role of intense weathering and postdepositional organic matter (OM) degradation on the Hg/TOC, show that post-depositional degradation of marine OM type II to type III may largely modify the amount and the quality of OM. The recorded Hg/TOC ratios may not reflect original Hg drawdown but postdepositional oxidation proxy in sediments. Therefore, the use of Hg to trace volcanism and critical geological events remains to be critically evaluated (Jin et al., 2022).

Consequently, we evaluated the total organic carbon (TOC, wt.%) content, mineral carbon (MinC, wt.%) content, hydrogen index (HI, mg HC/g TOC, HC = hydrocarbons), oxygen index (OI, mg CO_2/g TOC), and T_{max} (°C) as measured on powdered whole-rock sample using a Rock-Eval 6 (Behar et al., 2001) at the Institute of Earth Sciences of the University of Lausanne (ISTE–UNIL), Switzerland. Measurements were calibrated using the IFP160000 standard. T_{max} gives an estimate of the thermal maturation level of the organic matter (Behar et al., 2001). Pyrograms were carefully checked and HI values were not interpreted for TOC ≤0.2 wt.%, and T_{max} values for $S_2 \leq 0.3$ mg HC/g to avoid misinterpretation of flat thermograms. The analytical uncertainty was ±0.14%.

The relations between Hg and TOC, clay minerals (phyllosilicates) and pyrite have been evaluated (Figure 3) as Hg can be preferentially adsorbed on organic matter, hydrous iron oxides and pyrites, and/or clay minerals (e.g., Grasby et al., 2019; Percival et al., 2015; Sanei et al., 2012). This allows us to correctly evaluate the volcanic

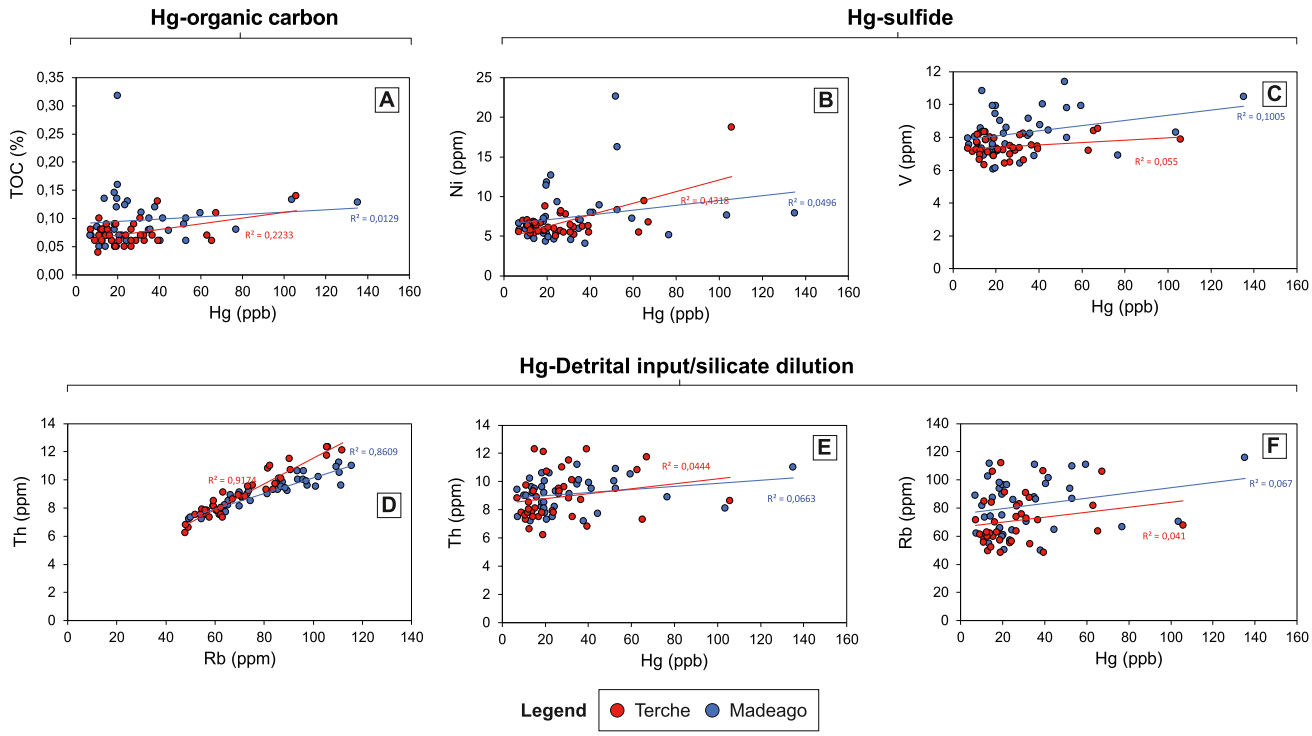

Figure 3. Binary plots of Hg content (ppb) versus TOC (%) and sulphide/detrital input tracers (ppm) as recorded at the Madeago (in blue) and Terche (in red) section sediments. Note the absence of a positive correlation between Hg/TOC, Hg/sulphides and Hg/detrital tracers at both sections. This supports the hypothesis of a volcanic source for the recorded Hg enrichments.

origin of the Hg anomalies present in the Terche and Madeago sections. Mercury has a strong affinity for organic matter (OM) in both marine and freshwater environments, reflected by significant Hg enrichments in organic-rich deposits in comparison to other sediments (Sanei et al., 2012). The Hg concentrations are therefore normalized against TOC contents in order to ensure that Hg enrichments are not directly related to increased OM accumulation and/or preservation (Percival et al., 2015). A significant correlation between Hg/TOC ratios and the raw Hg data indicate that the Hg enrichments are not related to changes in OM deposition alone (e.g., Grasby et al., 2019; Sanei et al., 2012).

Hg can also be related to detrital input and therefore diluted by silicate contents (e.g., clay minerals). Hg concentrations must be therefore normalized against Th or Rb in order to ensure that Hg enrichments are from volcanic origin and consequently not directly related to detrital input fluctuations or silicate dilution.

Trace element (TE) concentrations (ppm) were measured on pressed discs of powered samples and Mowiol II polyvinyl alcohol. Main elements (MEs) and TEs were analyzed by X-ray fluorescence spectrometry using a PANalytical PW2400 spectrometer of the Institute of Earth Sciences of the University of Lausanne (ISTE–UNIL), Switzerland. The detection limits are approx. 1–4 ppm for TEs. The accuracies of the analyses were assessed by analyses of standard reference materials.

3.2. Planktic Foraminifera and Radiolarians

A total of 40 samples were analyzed for their planktic foraminifera contents at Madeago spanning from −5.0 m to +3.0 m. The sample spacing varied from ∼2 to 10 cm across the MU and 30–60 cm below and above. As for the Terche section (D'Onofrio et al., 2016), foraminifera were extracted using the surfactant Neo-Steramina (alkyldimethylbenzylammonium chloride diluted at 10%).

Relative abundance of planktic foraminifera was obtained by counting the taxa in a population of about 300 specimens. Counts were performed on random splits of the washed residues from the ≥63 μm size fraction using a Micro Riffle Splitter Gilson SP-171X and expressed in percentage. The *Subbotina* group include the genera

Subbotina and *Parasubbotina* that were grouped according to their ecological affinities (e.g., Pearson et al., 2006, and references therein). The taxonomic criteria adopted in this study are the same as in D'Onofrio et al. (2016).

Radiolarian abundance at Madeago was estimated on 34 samples from the same interval investigated for planktic foraminifera. Radiolarian counts are expressed as percentage with respect to planktic foraminifera on a population of at least 300 specimens ($100 \times R/(R + P)$). However, the change in radiolarian relative abundance could be also driven by foraminiferal dilution, as our estimation of radiolarians is relative and not absolute abundance.

3.3. Calcareous Nannofossils

Fifty-six samples from the Madeago section were prepared from unprocessed material as smear slides and examined using a light microscope at ~1250X magnification. Samples for calcareous nannofossil analysis were collected at variable spacing (from 25 to 5 cm) to biostratigraphically characterize the section.

The presence or absence of index species was assessed via quantitative and semiquantitive analysis as by D'Onofrio et al. (2016). Specifically, (a) a prefixed number of taxonomically related forms was counted, that is, 30–100 *Sphenolithus* and *Discoaster*; and (b) specimens of biostratigraphically useful taxa but rare occurrence (i.e., *Discoaster* and *Tribrachiatus*) were counted in an area of about 6–7 mm^2, which is roughly equivalent to three vertical traverses.

To evaluate the abundance of paleoecologically relevant calcareous nannofossil groups, the taxa count was performed on at least 300 specimens and reported in percentages.

3.4. Calcareous Plankton Preservation and Dissolution Proxies

As dissolution of deep-sea carbonates related to the CCD/lysocline shallowing is often associated with early Eocene hyperthermals (e.g., Zachos et al., 2005), we evaluated possible bias on calcareous plankton assemblages due to carbonate dissolution by applying the same proxies adopted by D'Onofrio et al. (2016).

The F index was calculated like in D'Onofrio et al. (2016), as the ratio between fragments or partially dissolved planktic foraminiferal tests (showing notable deterioration, missing chambers or substantial breakage) versus entire tests on ~300 individuals.

The Plankton-Benthos ratio (P/B), is a widely adopted proxy for paleobathymetric estimations which in absence of significant bathymetric variations can be applied as a dissolution index (e.g., Nguyen et al., 2009). The P/B index was calculated on ~300 specimens and is expressed as ($100 \times P/(P + B)$).

The calcareous nannofossil Richness index simply indicates the number of taxa (species and genera). Besides evolution, it is influenced by dissolution and overgrowth.

The $T_{species}$ is the relative percentage of *Toweius* with a well-preserved central area (T_w) versus the total *Toweius*, including the poorly preserved forms (T_p) where the central area shows overgrowth or dissolution [%Tw/(% Tw + %Tp)]. High values indicate low dissolution.

The T/D ratio is the relative percentage of the dissolution prone *Toweius* over that of the dissolution resistant *Discoaster*. High values of T/D suggest low degree of dissolution.

3.5. Size Distribution Analyses

Planktic foraminiferal assemblage test size was determined on 39 samples from the Madeago section and on 27 samples from the Terche section using automated microscopy and the Olympus Stream Motion software at the University of Bristol, based on the methodologies in Schmidt et al. (2004). The test-size of planktic foraminiferal assemblages across the ETM2 at the southern Atlantic Site 1263 and tropical Pacific Site 1209 were evaluated following the same procedure described above (row data in Tables S9–S10 in Supporting Information S1). Samples were split to aliquots of 1000–1500 specimens on average, imaged at 160X magnification and the morphological parameters of each specimen were analyzed in Olympus Stream Motion. To remove juvenile specimens and lithic fragments from analyses, parameters were set to exclude particles with a maximum diameter smaller than 150 μm. Benthic foraminifera were removed via manual assessment. The 95th percentile of the maximum diameter was calculated for the remaining material (Schmidt et al., 2004) with an average measurement error of 1.75% or 8.10 μm (Todd et al., 2020).

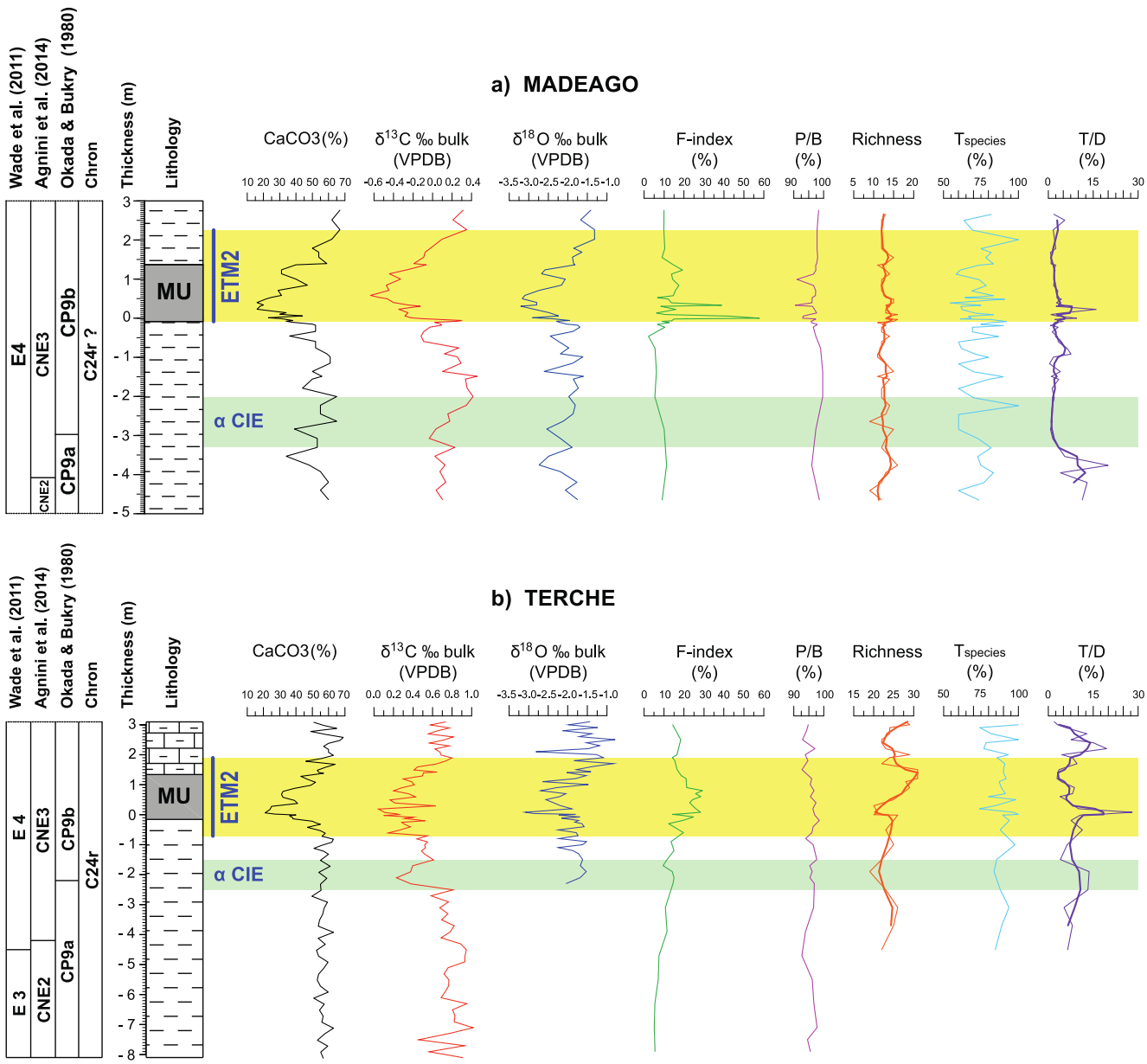

Figure 4. Foraminiferal and calcareous nannofossil dissolution proxies plotted alongside the carbon and oxygen stable-isotope record and the percentage of $CaCO_3$ at the Madeago (a) and Terche (b) sections. The dissolution indices based on foraminifera are the fragmentation index (F index) and the plankton benthos ratio (P/B). The dissolution proxies based on calcareous nannofossil are the taxa richness (Richness), the relative percentage of *Toweius* species with central area well preserved ($T_{species}$), and the *Toweius* (dissolution prone) *Discoaster* (dissolution resistant) ratio (T/D).

The same analysis was also performed on selected genera. About 150 specimens of *Morozovella*, *Acarinina*, *Subbotina* and *Chiloguembelina* were hand picked. However, *Subbotina* and *Chiloguembelina* are extremely rare in some samples across the ETM2 CIE interval making test size analysis impossible in some cases or referred to a reduced number of specimens (minimum: 30; on average: 100). The size data for the genus *Chiloguembelina* refer to the test length as it is characterized by an elongated test due to the biserial arrangement of chambers.

The calcareous nannofossil genera *Prinsius*, *Toweius* and *Ericsonia* produce small placoliths, that is, placoliths with sizes ≤3 μm, together with placoliths larger than 3 μm. As the increase in abundance of small placoliths may suggest a community size reduction, placoliths smaller than 3 μm were separated from placoliths larger than 3 μm for the cited genera. The abundance of both larger and small placholits of *Prinsius*, *Toweius* and *Ericsonia* were collected from the routine abundance counts (on ∼300 specimens).

4. Results and Preliminary Discussions

4.1. Tethyan Lithological and Stable Isotope Record of the ETM2

At the Madeago section the lowest $CaCO_3$ content (~16%) occurs within the MU at +0.23 m (Figure 2a, Table S1 in Supporting Information S1) synchronous with a negative Carbon Isotope Excursion (CIE) of ~0.9‰ (Figure 2, Table S1 in Supporting Information S1). The $\delta^{18}O$ record largely mirrors both the $CaCO_3$ and the $\delta^{13}C$ trends (Figure 2, Table S1 in Supporting Information S1) with a −3.2‰ excursion biostratigraphically correlated with the ETM2 event (Figure 2a). The $\delta^{13}C$ record below the ETM2 CIE is around a mean value of 0.15‰ and is not associated with any lithological changes with a negative excursion of −0.03‰, labeled as α CIE. The bulk carbon isotope trend of the ETM2 CIE at Madeago is comparable to bulk $\delta^{13}C$ patterns reported in literature (e.g., Cramer et al., 2003; Lourens et al., 2005; Stap et al., 2009).

The carbonate content and stable carbon and oxygen isotopes from the Terche section are provided by D'Onofrio et al. (2016) (Figure 2b). The $\delta^{13}C$ reduction of ~0.5‰, within the MU, is the isotopic expression of the ETM2 which correlates with the Madeago record. A negative $\delta^{13}C$ shift preceding the ETM2 is documented at Terche as well.

The $\delta^{18}O$ general profiles of the two studied sections appear depleted in the absolute values relative to marine calcite (e.g., Zachos et al., 2008) which we interpret as diagenetic alteration of the sediments driven by meteoric water (e.g., Schrag et al., 1995). We therefore do not discuss the lower part of $\delta^{18}O$ curve from the Terche section.

4.2. Variations in Geochemical Proxies and Evidence Supporting a Volcanic Source for Hg Spikes at Terche and Madeago

Three main increases of Hg/Th (or Hg/Rb) are recorded at Madeago within the α CIE, just below the ETM2 and at the base of ETM2 CIE (Figure 2a or Figure S1, Table S3 in Supporting Information S1). Increases of in As/Th-As/Rb, Pb/Th-Pb/Rb and Cr/Th-Cr/Rb also occur at the base of ETM2 CIE. At the Terche section, peaks of Hg/Th (or Hg/Rb) occur at the ETM2 base and above it (Figure 2b or Figure S2, Table S3 in Supporting Information S1).

In both Madeago and Terche sections, TOC contents are very low (Madeago: <0.32 wt%, mean value: 0.10wt%, Terche: <0.14wt%, mean value 0.07 wt%) and Hg cannot be normalized by TOC (Grasby et al., 2019). At Terche, Hg is not significantly correlated with TOC concentrations (R^2: 0.223, $n = 41$, Figure 3a). With one exception (sample TRE11 + 28), highest Hg values correspond to low TOC contents. TOC values are slightly higher at Madeago, but Hg contents are also not significantly correlated with TOC (R^2: 0.013, $n = 46$, Figure 3a). The highest TOC value (MAD 0: 0.32wt%) does not coincide with high Hg content (20 ppb). Hg enrichments are therefore not related to changes in organic matter deposition in both sections.

Trace element quantification is another way to evaluate the influence of pyrite (wt%) on the Hg distribution, since Ni, As, Cu, Mo are often linked with sulfide contents. At neither location is Ni correlated with Hg contents (Terche R^2: 0.432, $n = 41$; Madeago R^2: 0.049, $n = 47$; Figure 3b). Similarly, V shows no correlation with Hg (Terche, R^2: 0.055; Madeago, R^2: 0.101; Figure 3c). The absence of significant As enrichment in both sections is also a good indication of the absence of sulfides because FeS_2 pyrite commonly incorporates large amounts of arsenic (Wells & Mullens, 1973).

In both sections, the Hg is not significantly correlated with Th (Terche R^2: 0.066; Madeago, R^2: 0.044, Figure 3e) or Rb (Terche, R^2: 0.041; Madeago, R^2: 0.067; Figure 3f). This absence of correlation implies no significant terrestrial influx via detrital inputs (Grasby et al., 2019).

4.3. Excluding Taphonomic Bias in Calcareous Plankton Through Dissolution Proxies

The dissolution indicators show slight rises in dissolution at the base of the ETM2, albeit differently for different proxies (Figure 4a and Tables S4 and S5 in Supporting Information S1). Overall fragmentation is low with values of ~11%, increasing to 40% and 58% close to the onset of the ETM2 CIE but preceding its peak. Qualitatively, there is no dominance of a particular planktic foraminiferal genus among the fragmented tests. The binary plots of $CaCO_3$ content with the Fragmentation index show that there is no correlation (Figure S3 in Supporting Information S1). The P/B displays an overall mean value of ~97% with a minimum of 90.5% (Figure 4a), driven by slight dissolution as supported by the dissolution proxies.

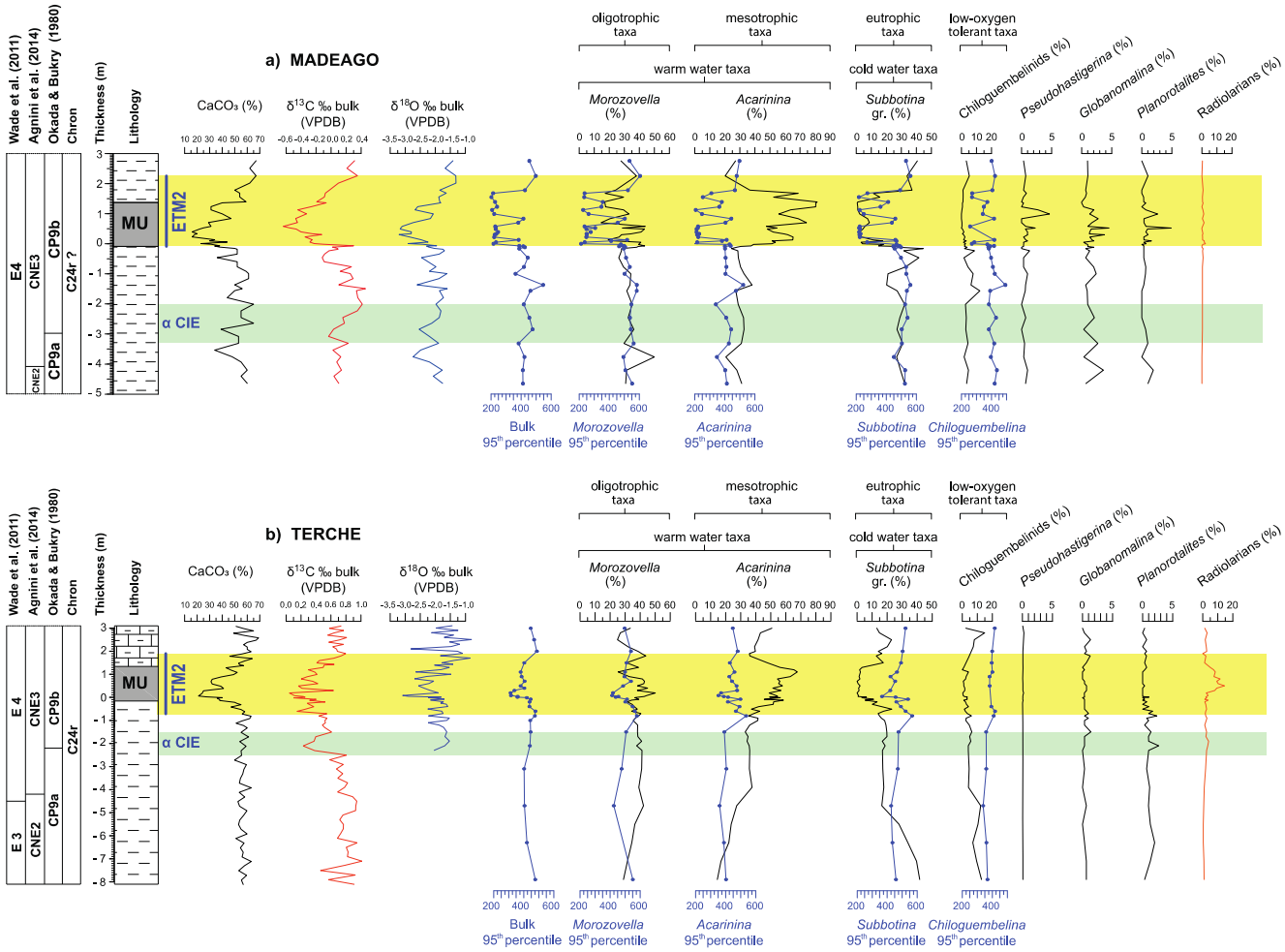

Figure 5. Variations 95th percentile of the maximum diameter of all individuals in the planktic foraminiferal assemblages, 95th percentile of maximum diameter of main genera (≥150 μm fraction) and relative abundance of planktic foraminiferal genera (≥63 μm fraction) and radiolarians across the Madeago (a) and Terche (b) sections. The *Subbotina* group includes the paleoecological similar genus, *Parasubbotina*.

The $T_{species}$ curve from Madeago shows values fluctuating from 100% to ∼60% (Figure 4b and Table S5 in Supporting Information S1) supporting minor dissolution. This is corroborated by low T/D (*Toweius* (dissolution prone)/*Discoaster* (dissolution resistant)) values of 3% with peaks of ∼10%–20% in the lower part of the section below the α CIE and at the base of the ETM2 CIE. The calcareous nannofossil based dissolution proxies do not show correlation with the $CaCO_3$ content (Figure S3 in Supporting Information S1).

Foraminiferal and nannofossil based dissolution proxies at Terche have been evaluated in D'Onofrio et al. (2016) (Figure 4b). The P/B suggest little change in dissolution whereas the F-index slightly increase (∼29%) close to the ETM2 CIE. Changes in calcareous nannofossil Richness index do not show evident correlation with the $CaCO_3$ and $\delta^{13}C$ pattern, with exception of the T/D proxy increases at the ETM2 as recorded at Madeago.

At the very base of ETM2 at Madeago an increase in foraminiferal dissolution is recorded. However, the synchronous increase of T/D values indicate a lower dissolution susceptibility in calcareous nannofossils.

4.4. Changes in Planktic Foraminiferal Assemblages and Radiolarian Abundance

Planktic foraminiferal assemblages at Madeago are dominated by the warm water mixed-layer dwellers *Acarinina* and *Morozovella* and the cold thermocline-dweller subbotinids (e.g., Boersma et al., 1987) (Figure 5a and Table S6 in Supporting Information S1). The genera *Pseudohastigerina*, *Globanomalina*, *Planorotalites*, and the low-oxygen tolerant taxa *Chiloguembelina* represent minor components of the assemblages (Figure 5a). Within the

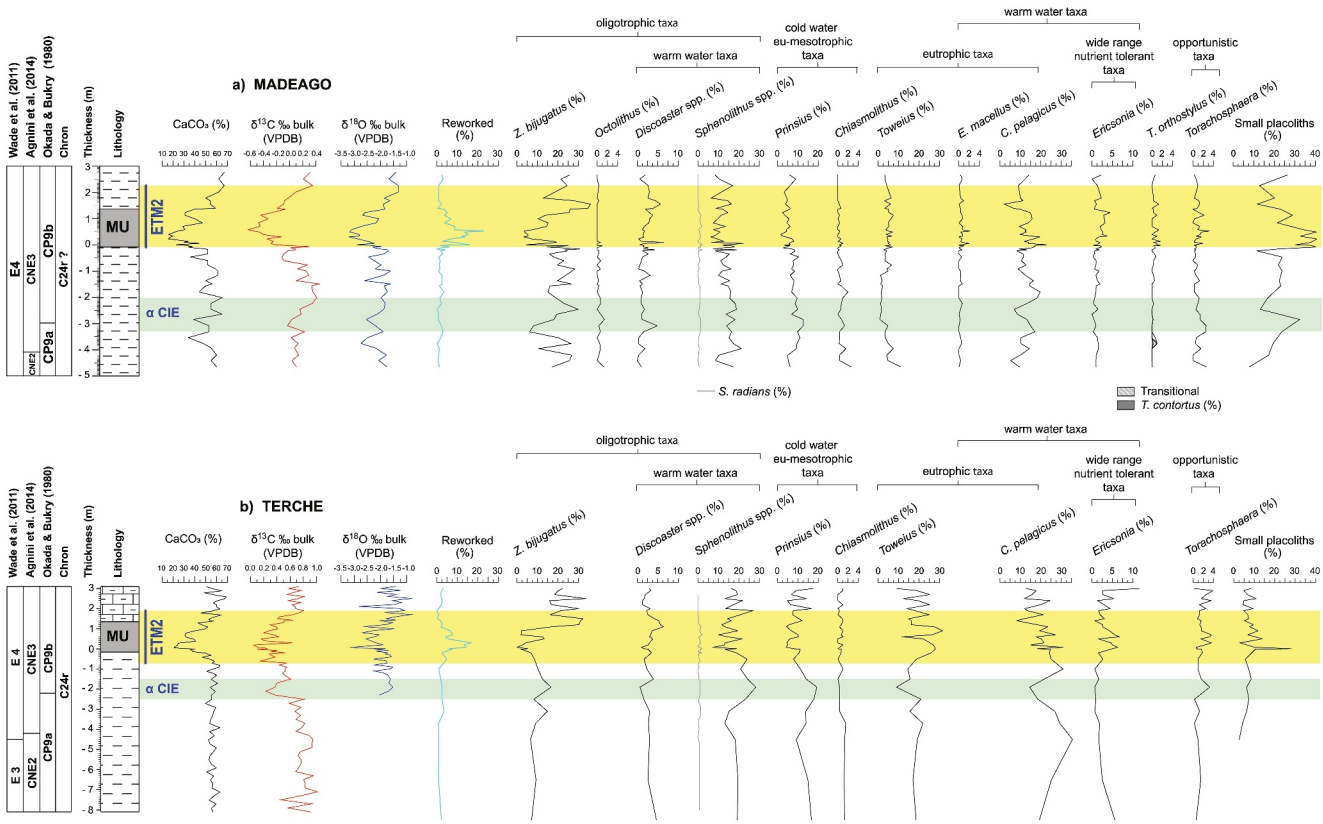

Figure 6. Variations in relative abundance of selected calcareous nannofossil taxa across the Madeago (a) and Terche (b) sections. The "small placoliths" include specimens of *Prinsius*, *Toweius* and *Ericsonia* with sizes ≤3 μm.

ETM2 *Acarinina* dominates the assemblage reaching 81.4% abundance whereas subbotinids and *Chiloguembelina* decline to 1% and 0% respectively, clearly showing the warming in the upper water column. The *Morozovella* abundances highly fluctuate within the ETM2, reaching peaks of ∼45% with minimum values of ∼15% at +0.700 m. These fluctuations are mainly out of phase with those recorded by *Acarinina*. Abundances are similar to those form the Terche section (Figure 5b).

At Madeago, radiolarians are rare throughout with a mean abundance of 0.5%. However, a slight increase up to ∼2% in abundance is recorded in the basal interval of the MU. At Terche, D'Onofrio et al. (2016) reported a major increase in radiolarian abundance within the MU up to ∼15% (Figure 5b).

4.5. Changes in Calcareous Nannofossils Assemblages

The calcareous nannofossil assemblages at Madeago are dominated by *Zygrhablithus bijugatus* (mean abundance more than 20%), *Coccolithus pelagicus*, *Sphenolithus* (mean abundance of ∼15% for each taxon) and small-size placoliths (mean abundance of ∼25%). Within the "normal-size" placoliths, *Prinsius* and *Toweius* account for 8% and 5%, respectively. The genus *Discoaster* is generally scarce except in the interval within the ETM2 where it peaks at 6%. The taxa *Chiasmolithus*, *Ericsonia*, *Tribrachiatus*, *Octolithus*, *Ellipsolithus macellus* and the calcareous dinocyst *Thoracosphaera* are minor components of the assemblage (Figure 6a and Table S8 in Supporting Information S1).

Calcareous nannofossil indices suggest general meso-oligotrophic conditions below the ETM2 interval but show striking modifications during the ETM2 CIE (Figure 6a) including a significant increase in the relative abundance of Cretaceous reworked taxa (up to ∼23%) (Figure 6a). Concomitantly with the peaks in Cretaceous specimens, oligotrophic taxa, such as *Discoaster*, *Sphenolithus*, *Z. bjiugatus* and *Octolithus* (e.g., Agnini et al., 2007; Gibbs et al., 2006), decrease their abundance (Figure 6a). In parallel, the genera *Thoracosphaera*, *Ericsonia*, *Toweius*, *E. macellus* and the species *C. pelagicus* significantly increase. These latter forms are known as meso/eutrophic

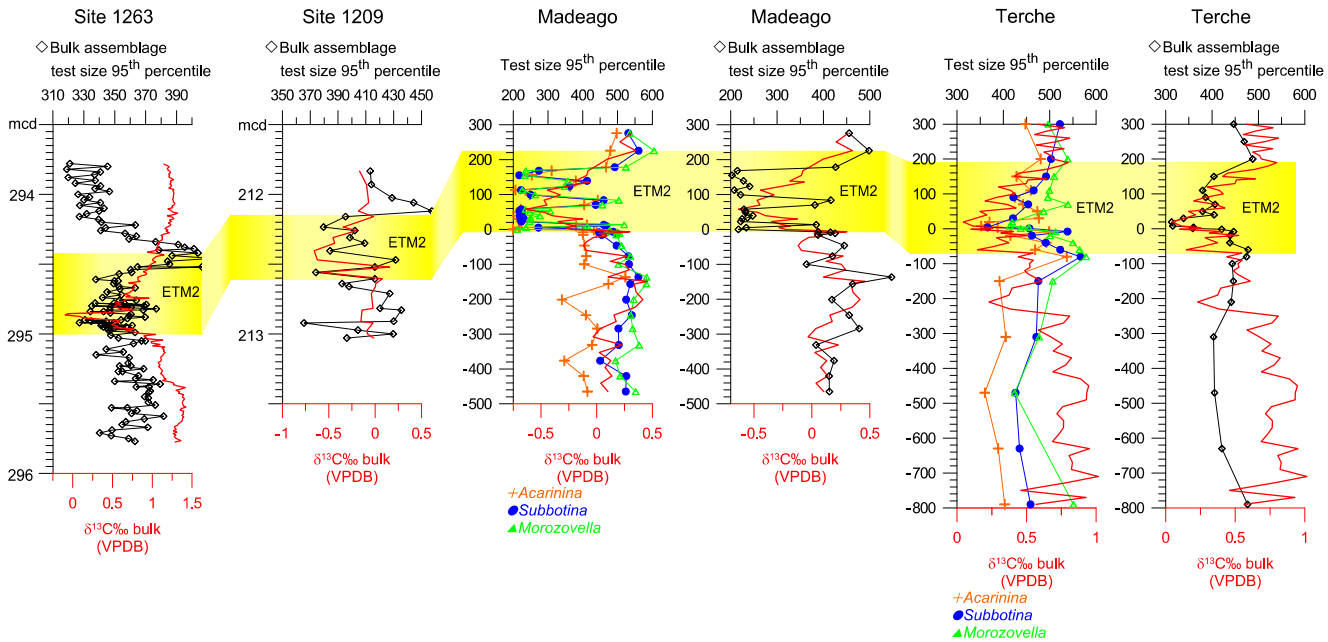

Figure 7. Planktic foraminiferal test-size of bulk assemblages from Sites 1263 (southern Atlantic) and 1209 (tropical Pacific) compared with sizes from Madeago and Terche across the ETM2. Stable isotope data are from Westerhold et al. (2018) (Site 1209) and Westerhold et al. (2020) (Site 1263).

indices (e.g., Agnini et al., 2007; Dedert et al., 2012). The oligotrophic *Discoaster* and *Z. bijugatus* display a marked recovery in abundance in the upper MU and throughout the $\delta^{13}C$ recovery. The cold-water genera *Prinsius* and *Chiasmolithus* show a slight general decrease from the onset of ETM2 CIE. The calcareous nannofossils proved to be more sensitive to the trophic conditions rather than temperature change and indicate a shift to eutrophic conditions at the ETM2.

The α CIE interval records complex changes in abundance. During the basal α CIE, oligotrophic taxa *Discoaster* decreases while *Z. bijugatus* increases. In the same interval the eutrophic *C. pelagicus* decreases and the cold index *Prinsius* show higher abundances as do "small placoliths." The α CIE recovery displays the opposite trend (Figure 6a). These recorded variations across the α CIE may suggest both cooler and oligotrophic conditions.

A similar overall distribution for calcareous nannofossil assemblages has been documented for the Terche section (D'Onofrio et al., 2016) (Figure 6b). The main differences are a significantly greater *Toweius* abundance at Terche than at Madeago (~20% vs. ~5%) and the small placoliths abundances which are higher at Madeago than at Terche (on average ~30% vs. ~6%).

4.6. Changes in Planktic Foraminiferal Test-Size

The test-size (95th percentile, $_{95/5}$) of planktic foraminifera collected from the open ocean sites varies across the event, but does not exceed background variability (Figure 7, Tables S9 and S10 in Supporting Information S1). As expected, the mean assemblage test size is slightly smaller at the mid latitude Site 1263 than at the tropical Site 1209. At Site 1209, across the ETM2 record mean test-size of the assemblage is ~400 μm, which is within error of the background values (~410 μm). At Site 1263 mean size is smaller during the ETM2 than pre-event values (360 vs. 394 μm). The minimum assemblage test-size at the ETM2 are 327 and 374 μm at Site 1263 and Site 1209 respectively, both of which are much larger than the minimum size (202 μm) at Madeago. At both sites, mean assemblage test-size increases either in the upper part or above the ETM2, at which size is larger than before (Figure 7, Tables S9 and S10 in Supporting Information S1). However, at Site 1263 size subsequently decreases to values lower than the pre-ETM2.

Below the CIE, foraminiferal test-size at Madeago has a mean value of 427 μm. This is broadly comparable to Site 1209, indicating a similarity to open ocean sites. In this interval, the largest test size is recorded by the genus *Morozovella* (average $_{95/5}$ size 527 μm), followed by *Subbotina* (average $_{95/5}$ size 507 μm), *Acarinina* (average $_{95/5}$

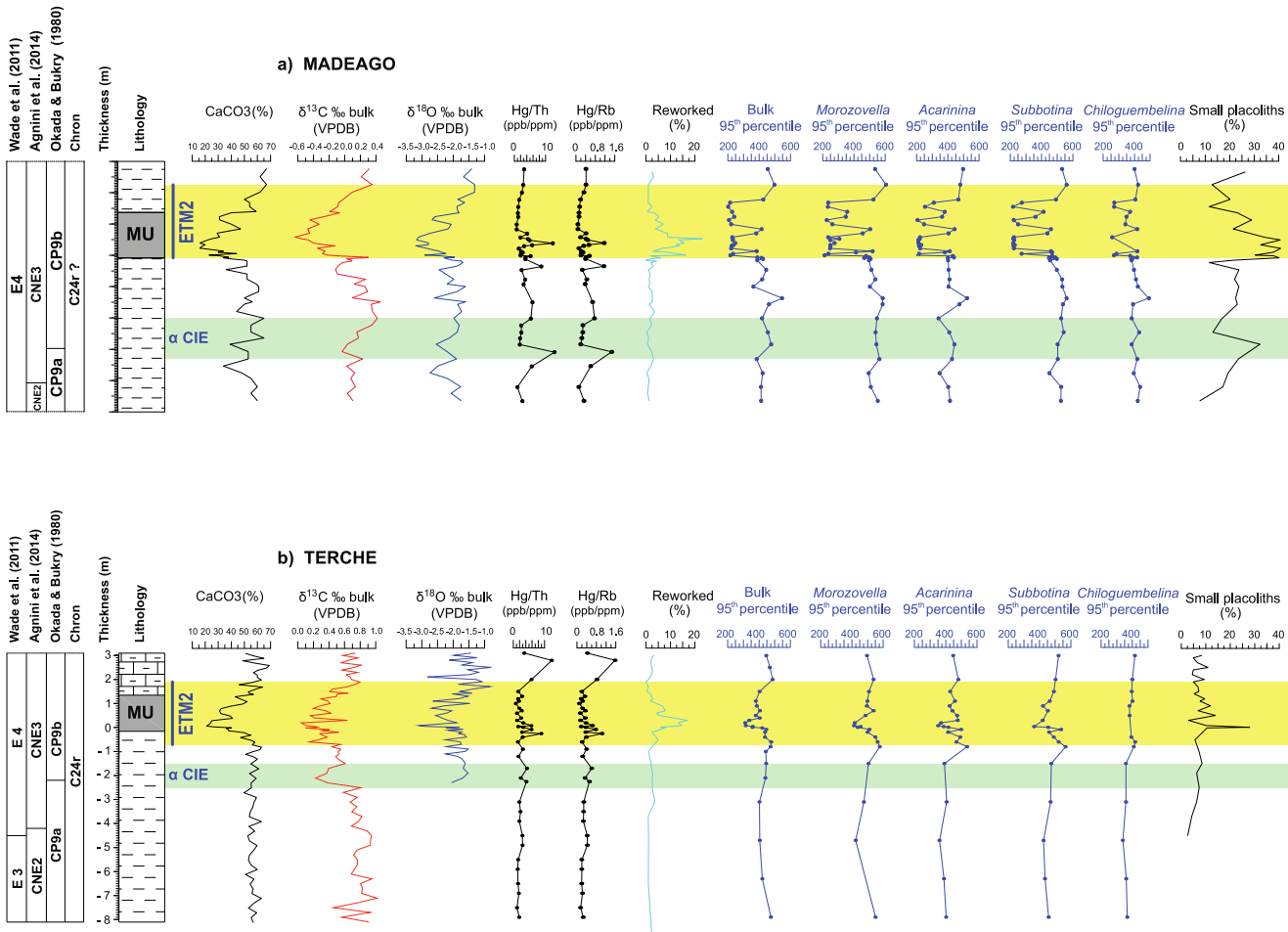

Figure 8. Planktic foraminiferal test-size (95th percentile) and abundance of "small placoliths" (<3 μm) of the genera *Prinsius*, *Toweius* and *Ericsonia* (%) curves shown alongside Cretaceous reworked calcareous nannofossils (%), Hg/Th, Hg/Rb (ppm) from Madeago (a) and Terche (b). Note that the increases of Hg/Th and Hg/Rb point to a volcanic origin of Hg. Note also that the levels recording Cretaceous reworked calcareous nannofossils do not coincide with the Hg peaks. The smallest planktic foraminiferal test-sizes and the higher percentage of "small placoliths" follow the Hg/Th and Hg/Rb increases.

size 416 μm) and *Chiloguembelina* (average $_{95/5}$ size 410 μm, note the strong linear extension of this taxon vs. the rounder nature of the other species). Size $_{95/5}$ was markedly lower (254 μm) within the ETM2 CIE, driven by a size reduction of *Acarinina (30%)*, *Morozovella* (~40%), *Subbotina* (~40%) (Figure 5a and Table S7 in Supporting Information S1). However, transient increases in mean foraminiferal size occur within the main CIE though never reaching the pre-event values. Interestingly, all the genera recovered their size above the CIE and even show their largest sizes (sizes $_{95/5}$ 460 μm) (Figure 5a and Table S7 in Supporting Information S1).

At Terche, the trend in test-size largely mirrors the Madeago record. Mean size $_{95/5}$ of 434 μm below the ETM2 CIE drops of ~100 μm within the main CIE. At Terche, decreases are smaller than at Madeago for individual taxa (Figure 5b and Table S7 in Supporting Information S1) resulting in a size reduction of ~20% for the genera investigated (Figure 5b and Table S7 in Supporting Information S1). A gradual recovery of planktic foraminiferal test-size occurs across the ETM2 CIE and post-CIE (Figure 5b and Table S7 in Supporting Information S1) where values higher than during the pre-ETM2 CIE interval are recorded. Notably, the test-size reduction follows the Hg peaks recorded below and at the ETM2 CIE base at both sections. No test-size decreases are recorded across the α CIE (Figure 8).

Dwarfism is not recorded for the genus *Chiloguembelina* at Terche and it is less pronounced compared to other genera at Madeago. However, these records may suffer from the reduced number of specimens analyzed due to the scarce abundance of this genus across the ETM2 interval. In addition, the increased dissolution at the ETM2

may have partly modified the record of chiloguembelinid size because their thin-walled test and biserial chambers make chiloguembelinids particularly prone to dissolution (Nguyen et al., 2011).

4.7. Changes in Calcareous Nannofossil Sizes

The abundance of "small placoliths" (<3 μm) in the genera *Prinsius*, *Toweius* and *Ericsonia* show significant variations in abundance at both sections (Figure 6 and Table S8 in Supporting Information S1). At Madeago, the most significant increase of "small placoliths" occurs at the ETM2 CIE until it declines during the ETM2 recovery. At the α CIE the "small placoliths" show a minor increase. The peaks observed at Madeago approximately follow the Hg/Rb-Hg/Th peaks (Figure 6). Within this general trend we observed three major peaks of small-size placoliths at 0.085/0.02 m, +0.092/+0.22 m and +0.49 and 1.12 m. At Terche "small placoliths" show a minor increase at the ETM2 MU, however, within the ETM2 interval we detected three peaks of "small placoliths" at +0.01 m, +0.50 m, and +0.90 m with the lowest peak reaching almost the 30% of assemblage. Interestingly at Madeago, this group shows a mean abundance almost five times greater than at Terche (~25% vs. ~6%).

5. Environmental Context Across the ETM2 and Drivers of Tethyan Calcareous Plankton Dwarfism

The main result of our study is the striking dwarfism of planktic foraminifera in the Tethyan realm across the ETM2 (Figures 5, 7, and 8). We infer a number of environmental stressors across this event which could induce dwarfing and have clear evidence that this dwarfing is not a taphonomic bias as indicated by minor variations in our dissolution proxies. The abundances of the calcareous plankton taxa support the existence of a stratified water column with a moderately expanded Oxygen Deficient Zone (ODZ) and a meso-oligotrophic mixed-layer before and after the ETM2. This is substantiated by the relative abundance of genera occupying diverse habitats, such as mixed-layer (*Acarinina*, *Morozovella*), thermocline (subbotinids) and ODZ (chiloguembelinids) (Figure 5) together with abundances of meso-oligotrophic indices within calcareous nannofossil assemblages (Figure 6).

We record significant environmental changes at the ETM2. The temperature increase as substantiated by our $\delta^{18}O$ data and globally recorded warming (e.g., Littler et al., 2014; Sluijs et al., 2009; Stap et al., 2009, 2010a,b) can explain the increase of planktic foraminiferal warm indices (mainly *Acarinina*) coupled with a decline in cold deep-dwellers (*Subbotina* and *Chiloguembelina*) (Figure 5). It is important to note that moderate carbonate dissolution during this interval may create some minor bias (Figure 4) as *Acarinina* is more resistant to dissolution than *Morozovella* and the subbotinids (Nguyen et al., 2011). However, spikes in *Acarinina* abundance across hyperthermal events are recorded from other successions where assemblages show low dissolution impact, that is, low F index (e.g., D'Onofrio et al., 2020; Luciani et al., 2017a, 2017b) therefore the increase of *Acarinina* concomitant with a decrease in subbotinids appears to be a genuine response to early Eocene warming. The warming therefore resulted in a migration of warm water taxa (mainly *Acarinina*) to our study location and a decline in cold deep-dwellers (*Subbotina* and *Chiloguembelina*) (Figure 5) akin to modern migrations in response to warming (e.g., Cooley et al., 2022).

Enhanced eutrophication via continental runoff is commonly associated with the intervals of marked warming in settings close to land due to an intensified hydrological cycle (e.g., Agnini et al., 2009; Giusberti et al., 2007, 2016). In our sections, eutrophication may have induced the increase in abundance of radiolarians (e.g., Hallock, 1987) and peaks in calcareous nannofossils eutrophic taxa (*C. pelagicus*, *Toweius* and *Thoracosphaera*) coupled with a drop in oligotrophic indices (*Discoaster*, *Sphenolithus*, *Z. bjiugatus* and *Octolithus*) (Figures 5 and 6). Eutrophication may have been responsible for the greater increase in the abundance of *Acarinina* than in the possibly more oligotrophic *Morozovella*, as recorded from other hyperthermals in similar settings (e.g., Agnini et al., 2009; D'Onofrio et al., 2016; Luciani et al., 2007). Importantly, across the PETM for the same setting (Forada section) where the eutrophication was much more intense, no dwarfism was recorded (Luciani et al., 2007).

A decrease in oxygenation during the ETM2 appears improbable due to increase in mixed layer taxa *Morozovella* and *Acarinina* which thrived in well-oxygenated environments. In addition, the decrease of chiloguembelinids (known to proliferate in the ODZ) exclude oxygen deficiency at the thermocline as recorded across the EECO (e.g., Luciani et al., 2020).

To evaluate potential drivers of the observed dwarfing, we have to consider that the environmental variability recorded in the Tethyan setting is different to the open ocean sites at which eutrophication during the ETM2 is not documented. Despite this, the different locations partially share the planktic foraminiferal response to global warming (with the exception of dwarfing). For example, at the Atlantic Sites 1258 and 1263 an increase of *Acarinina* and decrease of *Morozovella* and *Subbotina* is also recorded, though analyzed at a lower resolution (Luciani et al., 2017b; D'Onofrio et al., 2020), whereas at Shatsky Rise the variation in abundance of the two mixed-layer genera is reversed (Davis et al., 2022).

5.1. Excluding Evolutionary Control on Dwarfing and Summary of Dwarfing Cases in the Geological Record

Calcareous plankton size changes can be driven by evolutionary changes (e.g., Adebayo et al., 2023; Hallam, 1965; Rillo et al., 2020; Schmidt et al., 2006). The geologic record of reduction in the size of planktic foraminiferal tests is mainly linked to mass extinction (e.g., Luterbacher and Premoli Silva, 1964; Schmidt et al., 2006) often caused by the disappearance of the larger members within a group while dwarfed descendants or novel species flourish. The signal can be a combination of change in size of the dominant taxa as well as a reduction in abundance of the largest genera.

The dwarfing recorded in the Tethyan sections, though striking, cannot be ascribed to evolutionary modifications, in contrast to the PETM. During the PETM short lived excursion taxa (within the constraints of the morphospecies concept) and extinction of species changed the assemblages (e.g., Davis et al., 2022; Kelly et al., 1996; Pearson et al., 2006). Here in contrast, no extinction or new species are recorded during the ETM2 and the size change is constrained to the ETM2 and reversed afterward.

Variations in planktic foraminiferal size have also been related to highly stressed conditions and strong paleoenvironmental perturbations for example, at the latest Cenomanian Oceanic Anoxic Event 2 (OAE 2, Schlanger & Jenkyns, 1976) which records planktic foraminiferal dwarfism linked to high-surface productivity, low oxygen level and high pCO_2 (e.g., Coccioni & Luciani, 2005). Similar transient dwarfism has been recorded during multiple Mesozoic OAEs and interpreted as a response of new environmental conditions rather than evolution. Higher pCO_2 may have reduced calcification combined with an increase of nutrients resulting in higher abundances of nannoplankton producing small placoliths (e.g., Beaufort et al., 2011; Erba et al., 2019).

However, only few studies analyzed size variations on calcareous nannofossils across the Paleogene hyperthermals (e.g., Gibbs et al., 2013; Tremolada et al., 2008). These do not detect a change in *Discoaster multiradiatus* across the PETM despite above background variance in assemblage composition during the PETM, ETM2 and I1. Calcareous nannofossils do not record evolutionary modifications across the ETM2 in the Tethys (e.g., Agnini et al., 2007). During the Miocene, Mancini et al. (2021) show a significant size reduction in calcareous nannofossil taxa at the onset of the Messinian Salinity Crisis and link this to increased productivity and enhanced environmental variability, stimulating calcareous nannofossil growth rate and decreasing their platelet size.

The lack of dwarfism in planktic foraminifera and nannoplankton across a range of events (PETM, ETM2 and H2 at ODP Site 1209, Barrett et al., 2023; Davis et al., 2022) and our data from the Atlantic and Pacific oceans corroborates the lack of influence of evolutionary control and the uniqueness of the Tethyan record, possibly related to the local response to environmental stressors in the context of global warming.

5.2. Potential Environmental Stressors at the ETM2

Disentangling the environmental drivers for the observed dwarfism is difficult as the size reduction at the ETM2 is linked with changes in several environmental parameters for example, surface water warming and eutrophication, as discussed above.

Dwarfism may have been induced by enhanced metabolic rate in response to warming thus requiring more food to support growth (e.g., Gillooly et al., 2001). A strategy to optimize resource uptake is to enlarge surface area/volume ratio by reducing the cell mass and therefore the test size (e.g., Atkinson et al., 2003). O'Connor et al. (2009) demonstrated greater metabolic rates in heterotrophs compared to autotrophs. This evidence is consistent with the less pronounced dwarfism exhibited by calcareous nannofossils than by the planktic

foraminifera (Figures 5 and 6). However, this process cannot be the only cause of size reduction as it should have induced dwarfing in all the documented settings recording the ETM2 warming.

In addition, elevated ocean temperatures enhanced bacterial respiration thus resulting in more efficient recycling of nutrients higher in the water column (e.g., John et al., 2014). This would have restricted the food supply at depth which, together with warmer temperatures, might have led to a deterioration of the deeper dwelling niches occupied by chiloguembelinids and explain the virtual disappearance of this group in our sections across the ETM2 interval which would have also impacted subbotinids. A similar scenario has been proposed to account for the chiloguembelinid decline recorded at the Early Eocene Climatic Optimum (~53–49 Ma) from the Atlantic Ocean (Luciani et al., 2020). However, although this effect may explain changes in assemblages, it cannot be directly related to the observed size reduction.

Deoxygenation (Deutsch et al., 2022) is not a likely driver of dwarfing in our case, as the size reduction is also observed in mixed layer taxa, while deoxygenation of the upper water column is a feature commonly associated with the deep chlorophyl maximum at the thermocline (Oschlie et al., 2018). Nevertheless, the decreased abundance of chiloguembelinids at the ETM2 may suggest (beside the limited food resources) an increase in oxygen content rather than oxygen decrease at the ODZ (Luciani et al., 2020).

The increase in productivity recorded at the Madeago and Terche sections would have limited the growth of the oligotrophic symbiont bearing taxa, akin to observations in the modern ocean where the size of symbiont bearing taxa decreases toward the shore due to increases in productivity that reduces light availability (e.g., Ortiz et al., 1995). Nevertheless, symbiont bearing taxa (especially *Acarinina*) show an increase in our sections. In addition, this effect does not explain the size reduction in deeper dwelling taxa.

5.3. Indirect Impacts of Warming—Bleaching as a Cause of Dwarfism?

Symbiosis plays an important role in foraminiferal calcification and growth so photosymbiont loss (bleaching) may cause test-size reduction (e.g., Bé et al., 1982; Caron et al., 1982). In the modern ocean, symbiont bearing species are larger than non-symbiont bearing ones (Schmidt et al., 2004). High temperature is considered as the main factor inducing bleaching in recent benthic foraminifera (e.g., Hallock, 2000) and in the geological record of planktic foraminifera (Edgar et al., 2013; Luciani et al., 2017a). Therefore, the *Morozovella* and *Acarinina* test-size decrease in our record may have been driven by reduced symbiosis. However, Davis et al. (2022) did not find evidence of bleaching at the hyperthermals ETM2 and H2 for *Acarinina soldadoensis* and *Morozovella subbotinae* from the tropical Pacific Ocean (ODP Site 1209, Shatsky Rise) which, based on paleolatitude we infer as being even warmer than our locations. They argue that a critical environmental threshold was not reached in these lesser hyperthermals to induce bleaching. Lack of $\delta^{13}C$ data across different sizes for morozovellids and acarininids from our sections, which determines the presence or absence of photosymbiosis (e.g., Spero & DeNiro, 1987), prevents us from verifying this hypothesis. However, given that we also record a marked dwarfism in the asymbiotic genus, *Subbotina*, bleaching cannot be the only driver.

5.4. Possible Role of Biolimiting/Toxic Metals in Driving Local Size Reduction in Calcareous Plankton

Considering that the striking dwarfism recorded in our Tethyan sections appears atypical compared to the Pacific and Atlantic sites, we tentatively explore local drivers that could have been superimposed on the global warming. We speculate that toxic metals from submarine volcanic emissions could have impacted the calcareous plankton dwarfing across the ETM2 in the studied Tethyan sections. Volcanic derived proxies show an increase at the base of ETM2 in both sections (Figures 2, 5, 6, and 8). However, there is lack of direct temporal correlation between Hg/Th and Hg/Rb ratios and bulk assemblage and genus sizes, as shown in Figure S4 in Supporting Information S1. It is worth to notice that the residence times of mercury following an input pulse in surface ocean waters, suggest relatively rapid removal within hundreds of years, as highlighted by modeling studies (Amos et al., 2013). Nevertheless, it is important to consider that, while the majority of mercury may be removed from the surface oceans within hundreds of years, a fraction may persist in deep ocean reservoirs or be recycled through biological and geochemical processes within marine ecosystems. This persistent presence of trace amounts of mercury could contribute to long-term ecological effects, even after the initial input pulse has dissipated (e.g., Lamborg et al., 2014; Mason & Sheu, 2002; Sunderland et al., 2009).

In summary, our speculation considers that, while there may not be a direct link between volcanic emissions and dwarfing, other indirect mechanisms related to the long-term effects of volcanism on ocean chemistry and biology may have contributed to the observed patterns. However, further investigation is needed to improve our understanding of the indirect links between volcanism and ecosystem responses, including dwarfing events.

The volcanic input at Terche and Madeago was likely derived from the nearby submarine emissions of the Veneto Volcanic Province (Figure 1), which was active from the late Paleocene to the late Oligocene (Brombin et al., 2021 and references therein). According to Papazzoni et al. (2014) geological evidence of volcanic activity is present at Spilecco (~98 km southwest of the studied sections) and is constrained within the lower Eocene calcareous nannofossil Zones NP10-NP12/planktic foraminiferal Zone E2-E5 (from ~55.4 Ma to ~ 51 Ma). The Cretaceous nannofossil reworking and terrigenous dilution at the ETM2, indicating enhanced continental weathering triggered by an accelerated hydrological cycle, did not cause element re-sedimentation in our sections as supported by the negative correlation in the binary plots of Hg with the elements considered as tracers of detrital input (Figure 2 and Table S3 in Supporting Information S1). Furthermore, the Hg peak during the ETM2 CIE does not coincide with the Cretaceous reworked levels (Tables S3 and S8 in Supporting Information S1). The sole evidence of volcanic emission in our sections is given by the Hg/Th-Hg/Rb increase as no ash horizons are present.

The understanding of the impacts of volcanism on the ocean's planktic ecosystem are still in their infancy, even in the modern ocean (Bisson et al., 2023). Experiments have shown the potential release of biolimiting micronutrients from volcanic sources may stimulate productivity (Jones & Gislason, 2008). At the same time, in experimental settings the addition of volcanic ash and resultant release of elevated trace metals reduced growth of the modern coccolithphore *E. huxleyi* and *C. pelagicus* though not all taxa were impacted (Faucher et al., 2017; Hoffmann et al., 2012). Laboratory experiments on controlled exposure of trace metals (Zn, Cu, Pb, Hg) are almost exclusively focused on benthic foraminifera in polluted systems with high concentrations of these element (e.g., Frontalini et al., 2018 and references therein; Nigam et al., 2006). In specimens of the benthic *Rosalina leei* subjected to inorganic mercury ($HgCl_2$ dissolved in seawater) the growth rate and maximum size decreased considerably (Nigam et al., 2009; Saraswat et al., 2004). Specimens of *Globorotalia menardii* extracted from the Young Toba Tuff layer (74,000 years ago) show incorporation of trace metals in the wall but no test-size reduction (Lemelle et al., 2020). As planktic foraminifera from ETM2 are all extinct forms we cannot evaluate a possible negative impact of trace metals on their test-size. In addition, test preservation of Madeago and Terche foraminifera (recrystallized and infilled) prevents to verify the possible incorporation of trace elements in the foraminiferal tests.

In conclusion, considering that warming and eutrophication alone cannot explain the striking size reduction, we speculate that the volcanic input of toxic metals could have acted synergistically to induce dwarfing hence explaining the uniqueness of our findings.

We tentatively explain the greater dwarfism at the ETM2 at Madeago as well as differences in calcareous plankton abundance of genera, compared to the nearby location of Terche, with the complex paleogeography of the area. The Alpine-Dinaric tectonic activity uplifted blocks previously deposited in deep sea settings at shallower depth through complex transpressive mechanisms (e.g., Bosellini, 1989; Luciani, 1989). We suppose that these blocks may have controlled the local distribution of elements and partly sheltered Terche from volcanic sources, thus potentially explaining the minor effect of dwarfism at Terche. These blocks may have also controlled the pattern of currents rich in nutrient input from land thus justifying the greater eutrophication at the same section. Unfortunately, detailed paleogeographic reconstructions are not available for the area (Luciani, 1989), so it is also impossible to establish potential diverse palaeodistances of the two sections from the shore line.

6. Summary and Conclusions

The ETM2 environmental perturbation impacted calcareous plankton at the studied Tethyan setting, with modified assemblages uniquely resulting in planktic foraminiferal dwarfism (up to ~40% decrease in test size compared to pre-event values) at Madeago and Terche. We attribute the greater test size reduction at Madeago than at Terche to local oceanography.

Together, our data suggest that the environmental changes impacted planktic foraminifera more than coccolithophores, but that both plankton types exhibit resilience as they recover previous size and composition of communities after the ETM2 disturbance.

The marked foraminiferal dwarfism at the studied Tethyan location is unusual compared to literature and our open ocean data. As the marked test-size reduction involved both surface and deeper dwellers, parameters impacting the upper water column, such as deoxygenation or warming are not likely drivers. Furthermore, the ETM2 is characterized by a *global* increase in sea surface temperature and therefore cannot explain the unique dwarfism. Eutrophication in our setting, though not detected in open ocean areas, cannot alone justify the size reduction as no dwarfing was recorded across the extreme warming of the PETM in the same geological setting that was characterized by greater eutrophy.

The Hg peaks occurring just below and at the ETM2 onset suggest an increase in toxic metals, associated with coeval volcanic activity. In contrast, size reduction is not observed in other stratigraphic intervals with Hg peaks (below and above the ETM2) where oxygen isotope data do not show warm conditions. As such, we speculate that a combination of regional and global processes (e.g., increased toxic metals alongside warming) may have acted additively to induce dwarfism. Our speculation emphasizes the need for studies that evaluate the effect of toxic elements from volcanic emissions (including the concentration and duration of emission pulse) on planktic foraminifera.

Conflict of Interest

The authors declare no conflicts of interest relevant to this study.

Data Availability Statement

Data set for this study are archived in the Pangea repository and are available as .xlsx and html format at D'Onofrio et al. (2024).

Acknowledgments

We are very grateful to Editor Ursula Röhl, to the reviewer Marlow J. Cramwinckel and to the anonymous reviewers for their constructive comments that gave us the opportunity to greatly improved the scientific content of the paper and its clarity and readability. Work funded by MIUR-PRIN 2017 "Biotic Resilience to Global Change" Grant 80007370382, FAR (Fondo Ateneo Ricerca, Ferrara University) 2021 and FIRD 2024 to V.L., D.S. was funded via NERC Grant NE/P019439/1. E.F. and L.G. have been funded by R.D.O. fundings (ex 60%) of the University of Padova. We are grateful to Tiffany Monnier and Olivier Reubi (ISTE, Lausanne University) for their help in the TOC and Hg analyses and for the XRF trace analyses respectively.

References

Adebayo, M. B., Bolton, C. T., Marchant, R., Bassinot, F., Conrod, S., & de Garidel-Thoron, T. (2023). Environmental controls of size distribution of modern planktonic foraminifera in the Tropical Indian Ocean. *Geochemistry, Geophysics, Geosystems*, *24*(4), e2022GC010586. https://doi.org/10.1029/2022GC010586

Agnini, C., Fornaciari, E., Raffi, I., Catanzariti, R., Pälike, H., Backman, J., & Rio, D. (2014). Biozonation and biochronology of Paleogene calcareous nannofossils from low and middle latitudes. *Newsletters on Stratigraphy*, *47*(2), 131–181. https://doi.org/10.1127/0078-0421/2014/004

Agnini, C., Fornaciari, E., Rio, D., Tateo, F., Backman, J., & Giusberti, L. (2007). Responses of calcareous nannofossil assemblages, mineralogy and geochemistry to the environmental perturbations across the Paleocene/Eocene boundary in the Venetian pre-Alps. *Marine Micropaleontology*, *63*(1–2), 19–38. https://doi.org/10.1016/j.marmicro.2006.10.002

Agnini, C., Macrì, P., Backman, J., Brinkhuis, H., Fornaciari, E., Giusberti, L., et al. (2009). An early Eocene carbon cycle perturbation at ~52.5 Ma in the Southern Alps: Chronology and biotic response. *Paleoceanography*, *24*(2), PA2209. https://doi.org/10.1029/2008PA001649

Amos, H. M., Jacob, D. J., Streets, D. G., & Sunderland, E. M. (2013). Legacy impacts of all-time anthropogenic emissions on the global mercury cycle. *Global Biochemical Cycles*, *27*(2), 410–421. https://doi.org/10.1002/gbc.20040

Atkinson, D., Ciotti, B. J., & Montagnes, D. J. S. (2003). Protists decrease in size linearly with temperature ca. 2.5% $°C^{-1}$. *Proceedings of the Royal Society of London. Series B*, *270*(1533), 2605–2611. https://doi.org/10.1098/rspb.2003.2538

Barrett, R., Adebowale, M., Birch, H., Wilson, J. D., & Schmidt, D. N. (2023). Planktic foraminiferal resilience to environmental change associated with the PETM. *Paleoceanography and Paleoclimatology*, *38*(8), e2022PA004534. https://doi.org/10.1029/2022PA004534

Bé, A. W. H., Spero, H. J., & Anderson, O. R. (1982). Effect of symbiont elimination and reinfection on the life processes of the planktonic foraminifera *Globigerinoides sacculifer*. *Marine Biology*, *70*(1), 73–86. https://doi.org/10.1007/BF00397298

Beaufort, L., Probert, I., de Garidel-Thoron, T., Bendif, E. M., Ruiz-Pino, D., Metzl, N., et al. (2011). Sensitivity of coccolithophores to carbonate chemistry and ocean acidification. *Nature*, *476*(7358), 80–83. https://doi.org/10.1038/nature10295

Behar, F., Beaumont, V., & Penteado, H. L. D. (2001). Rock-eval 6 technology: Performances and developments. *Oil and Gas Science and Technology*, *56*(2), 111–134. https://doi.org/10.2516/ogst:2001013

Bisson, K. M., Gassó, S., Mahowald, N., Wagner, S., Koffman, B., Carn, S. A., et al. (2023). Observing ocean ecosystem responses to volcanic ash. *Remote Sensing of Environment*, *296*, 113749. https://doi.org/10.1016/j.rse.2023.113749

Boersma, A., Premoli Silva, I., & Shackleton, N. (1987). Atlantic Eocene planktonic foraminiferal biogeography and stable isotopic paleoceanography. *Paleoceanography*, *2*(3), 287–331. https://doi.org/10.1029/pa002i003p00287

Bosellini, A. (1989). Dynamics of Tethyan carbonate platform. *SEPM Society for Sedimentary Geology*, *44*, 3–13. https://doi.org/10.2110/pec.89.44

Brombin, V., Pettitt, E. A., Fahnestock, M. F., Casalini, M., Webb, L. E., Bryce, J. G., & Bianchini, G. (2021). New geochemical and geochronological data on the Cenozoic Veneto Volcanic Province: Geodynamic inferences. *Lithos*, *406–407*, 106507. https://doi.org/10.1016/j.lithos.2021.106507

Capdevila, P., Stott, I., Beger, M., & Salguero-Gómez, R. (2020). Towards a comparative framework of demographic resilience. *Trends in Ecology & Evolution*, *35*(9), 776–786. https://doi.org/10.1016/j.tree.2020.05.001

Caron, D. A., Bé, A. W. H., & Anderson, O. R. (1982). Effects of variations in light intensity on life processes of the planktonic foraminifer *Globigerinoides sacculifer* in laboratory culture. *Journal of the Marine Biological Association of the United Kingdom*, *62*(2), 435–451. https://doi.org/10.1017/S0025315400057374

Charbonnier, G., Adatte, T., Föllmi, K. B., & Suan, G. (2020). Effect of intense weathering and postdepositional degradation of organic matter on hg/toc proxy in organic-rich sediments and its implications for deep-time investigations. *Geochemistry, Geophysics, Geosystems*, *21*(2), e2019GC008707. https://doi.org/10.1029/2019gc008707

Coccioni, R., & Luciani, V. (2005). Planktonic foraminifers across the Bonarelli Event (OAE2, latest Cenomanian): The Italian record. *Palaeogeography, Palaeoclimatology, Palaeoecology*, *224*(1–3), 167–185. https://doi.org/10.1016/j.palaeo.2005.03.039

Cooley, S. R., Schoeman, D. S., Bopp, L., Boyd, P. W., Donner, S. D., et al. (2022). Ocean and coastal ecosystems and their services. In H.-O. Pörtner, D. C. Roberts, M. Tignor, E. S. Poloczanska, K. Mintenbeck, et al. (Eds.), *Climate change 2022: Impacts, adaptation and vulnerability; contribution of working group II to the sixth assessment report of the intergovernmental panel on climate change*. Cambridge Univ. Press.

Cramer, B. S., Kent, D. V., & Aubry, M.-P. (2003). Orbital climate forcing of excursions in the late Paleocene–early Eocene (chrons C24n–C25n). *Paleoceanography*, *18*(4), 1097. https://doi.org/10.1029/2003PA000909

Davis, C. V., Shaw, J. O., D'haenens, S., Thomas, E., & Hull, P. M. (2022). Photosymbiont associations persisted in planktic foraminifera during early Eocene hyperthermals at Shatsky Rise (Pacific Ocean). *PLoS One*, *17*(9), e0267636. https://doi.org/10.1371/journal.pone.0267636

Dedert, M., Stoll, H. M., Kroon, D., Shimizu, N., Kanamaru, K., & Ziver, P. (2012). Productivity response of calcareous nannoplankton to Eocene Thermal Maximum 2 (ETM2). *Climate of the Past*, *8*(3), 977–993. https://doi.org/10.5194/cp-8-977-2012

Deutsch, C., Penn, J. L., Verberk, W. C. E. P., Inomura, K., Endress, M.-G., & Payne, J. L. (2022). Impact of warming on aquatic body sizes explained by metabolic scaling from microbes to macrofauna. *Proceedings of the National Academy of Sciences of the United States of America*, *119*(28), e2201345119. https://doi.org/10.1073/pnas.2201345119

Dickens, G. R. (2011). Down the rabbit hole: Toward appropriate discussion of methane release from gas hydrate systems during the Paleocene–Eocene Thermal Maximum and other past hyperthermal events. *Climate of the Past*, *7*(3), 831–846. https://doi.org/10.5194/cp-7-831-2011

D'Onofrio, R., Barrett, R., Schmidt, D. N., Fornaciari, E., Giusberti, L., Frijia, G., et al. (2024). Extreme planktic foraminiferal dwarfism across the ETM2 in the Tethys Realm in response to warming [dataset bundled publication] [Dataset]. *PANGAEA*. https://doi.org/10.1594/PANGAEA.967574

D'Onofrio, R., Luciani, V., Dickens, G. R., Wade, B. S., & Kirtland-Turner, S. (2020). Demise of the planktic foraminifer genus morozovella during the early Eocene climatic optimum: New records from ODP site 1258 (Demerara Rise, Western Equatorial Atlantic) and site 1263 (Walvis Ridge, South Atlantic). *Geosciences*, *10*(3), 88. https://doi.org/10.3390/geosciences10030088

D'Onofrio, R., Luciani, V., Fornaciari, E., Giusberti, L., Galazzo, F. B., Dallanave, E., et al. (2016). Environmental perturbations at the early Eocene ETM2, H2, and I1 events as inferred by Tethyan calcareous plankton (Terche section, northeastern Italy) [Dataset]. *Paleoceanography*, *31*,(9), 1225–1247. https://doi.org/10.1002/2016PA002940

Edgar, K. M., Paelike, H., & Wilson, P. A. (2013). Testing the impact of diagenesis on the delta O-18 and delta C-13 of benthic foraminiferal calcite from a sediment burial depth transect in the equatorial Pacific. *Paleoceanography*, *28*(3), 468–480. https://doi.org/10.1002/palo.20045

Erba, E., Bottini, C., Faucher, G., Gambacorta, G., & Visentin, S. (2019). The response of calcareous nannoplankton to Oceanic Anoxic Events: The Italian pelagic record. *Bollettino della Societa Paleontologica Italiana*, *58*, 51–71. https://doi.org/10.4435/BSPI.2019.08

Faucher, G., Hoffmann, L., Bach, L. T., Bottini, C., Erba, E., & Riebesell, U. (2017). Impact of trace metal concentrations on coccolithophore growth and morphology: Laboratory simulations of Cretaceous stress. *Biogeosciences*, *14*(14), 3603–3613. https://doi.org/10.5194/bg-14-3603-2017

Font, E., Chen, J., Regelous, M., Regelous, A., & Adatte, T. (2022). Volcanic origin of the mercury anomalies at the Cretaceous-Paleogene transition of Bidart, France. *Geology*, *50*(2), 142–146. https://doi.org/10.1130/G49458.1

Frieling, J., Mather, T. A., März, C., Jenkyns, H. C., Hennekam, R., Reichart, G.-J., et al. (2023). Effects of redox variability and early diagenesis on marine sedimentary Hg records. *Geochimica et Cosmochimica Acta*, *351*, 78–95. https://doi.org/10.1016/j.gca.2023.04.015

Frontalini, F., Nardelli, M. P., Curzi, D., Martín-González, A., Sabbatini, A., Negri, A., et al. (2018). Benthic foraminiferal ultrastructural alteration induced by heavy metals. *Marine Micropaleontology*, *138*, 83–89. https://doi.org/10.1016/j.marmicro.2017.10.009

Gibbs, S. J., Bown, P. R., Murphy, B. H., Sluijs, A., Edgar, K. M., Pälike, H., et al. (2012). Scaled biotic disruption during early Eocene global warming events. *Biogeosciences*, *9*(11), 4679–4688. https://doi.org/10.5194/bg-9-4679-2012

Gibbs, S. J., Bralower, T. J., Bown, P. R., Zachos, J. C., & Bybell, L. M. (2006). Shelf and open ocean calcareous phytoplankton assemblages across the Paleocene–Eocene thermal maximum: Implications for global productivity gradients. *Geology*, *34*(4), 233–236. https://doi.org/10.1130/G22381.1

Gibbs, S. J., Poulton, A. J., Bown, P. R., Daniels, C. J., Hopkins, J., Young, J. R., et al. (2013). Species-specific growth response of coccolithophores to Palaeocene-Eocene environmental change. *Nature Geoscience*, *6*(3), 218–222. https://doi.org/10.1038/ngeo1719

Gillooly, J. F., Brown, J. H., West, G. B., Savage, V. M., & Charnov, E. L. (2001). Effects of size and temperature on metabolic rate. *Science*, *293*(5538), 2248–2251. https://doi.org/10.1126/science.1061967

Giusberti, L., Boscolo Galazzo, F., & Thomas, E. (2016). Variability in climate and productivity during the Paleocene–Eocene Thermal Maximum in the western Tethys (Forada section). *Climate of the Past*, *12*(2), 213–240. https://doi.org/10.5194/cp-12-213-2016

Giusberti, L., Rio, D., Agnini, C., Backman, J., Fornaciari, E., Tateo, F., & Oddone, M. (2007). Mode and tempo of the Paleocene-Eocene thermal maximum in an expanded section from the Venetian pre-Alps. *GSA Bulletin*, *119*(3–4), 391–412. https://doi.org/10.1130/B25994.1

Grasby, S. E., Them, T. R., Chen, Z., Yin, R., & Ardakani, O. H. (2019). Mercury as a proxy for volcanic emissions in the geologic record. *Earth-Science Reviews*, *196*, 102880. https://doi.org/10.1016/j.earscirev.2019.102880

GutjahrRidgwell, M. A., Sexton, P. F., Anagnostou, E., Pearson, P. N., Pälike, H., Norris, R. D., et al. (2017). Very large release of mostly volcanic carbon during the Palaeocene–Eocene Thermal Maximum. *Nature*, *548*(7669), 573–577. https://doi.org/10.1038/nature23646

Hallam, A. (1965). Environmental causes of stunting in living fossil marine benthonic invertebrates. *Palaeontology*, *8*, 132–155.

Hallock, P. (1987). Fluctuations in the trophic resource continuum: A factor in global diversity cycles? *Paleoceanography*, *2*(5), 457–471. https://doi.org/10.1029/PA002i005p00457

Hallock, P. (2000). Symbiont-bearing foraminifera: Harbingers of global change? *Micropaleontology*, *46*, 95–104.

Hodgson, D., McDonald, J. L., & Hosken, D. J. (2015). What do you mean, resilient. *Trends in Ecology & Evolution*, *30*(9), 503–506. https://doi.org/10.1016/j.tree.2015.06.010

Hoffmann, L. J., Breitbarth, E., Ardelan, M. V., Duggen, S., Olgun, N., Hassellöv, M., & Wängberg, S. Å. (2012). Influence of trace metal release from volcanic ash on growth of Thalassiosira pseudonana and Emiliania huxleyi. *Marine Chemistry*, *132–133*, 28–33. https://doi.org/10.1016/j.marchem.2012.02.003

Holbourn, A., Henderson, A. S., & MacLeod, N. (2013). *Atlas of benthic foraminifera* (p. 642). Wiley-Blackwell.

Jennions, S. M., Thomas, E., Schmidt, D. N., Lunt, D., & Ridgwell, A. (2015). Changes in benthic ecosystems and ocean circulation in the Southeast Atlantic across Eocene Thermal Maximum 2. *Paleoceanography*, *30*(8), 1059–1077. https://doi.org/10.1002/2015PA002821

Jin, S., Kemp, D. B., Yin, R., Sun, R., Shen, J., Jolley, D. W., et al. (2023). Mercury isotope evidence for protracted North Atlantic magmatism during the Paleocene-Eocene Thermal Maximum. *Earth and Planetary Science Letters*, *602*, 117926. https://doi.org/10.1016/j.epsl.2022.117926

Jin, X., Ogg, J. G., Lu, S., Shi, Z., Kemp, D. B., Hua, X., et al. (2022). Terrestrial record of carbon-isotope shifts across the Norian/Rhaetian boundary: A high-resolution study from northwestern Sichuan Basin, South China. *Global and Planetary Change*, *210*, 103754. https://doi.org/10.1016/j.gloplacha.2022.103754

John, E. H., Wilson, J. D., Pearson, P. N., & Ridgwell, A. (2014). Temperature-dependent remineralization and carbon cycling in the warm Eocene oceans. *Palaeogeography and Palaeoclimatology*, *413*, 158–166. https://doi.org/10.1016/j.palaeo.2014.05.019

Jones, M. T., & Gislason, S. R. (2008). Rapid releases of metal salts and nutrients following the deposition of volcanic ash into aqueous environments. *Geochimica et Cosmochimica Acta*, *72*(15), 3661–3680. https://doi.org/10.1016/j.gca.2008.05.030

Kelly, D. C., Bralower, T. J., Zachos, J. C., Premoli-Silva, I., & Thomas, E. (1996). Rapid diversification of planktonic foraminifera in the tropical Pacific (ODP Site 865) during the late Paleocene thermal maximum. *Geology*, *24*(5), 423–426. https://doi.org/10.1130/0091-7613(1996)024<0423:rdopfi>2.3.co;2

Kirtland-Turner, S., Sexton, P. F., Charled, C. D., & Norris, R. D. (2014). Persistence of carbon release events through the peak of early Eocene global warmth. *Nature Geoscience*, *7*(10), 748–751. https://doi.org/10.1038/NGEO2240

Lamborg, C. H., Hammerschmidt, C. R., Bowman, K. L., Swarr, G. J., Munson, K. M., Ohnemus, D. C., et al. (2014). A global ocean inventory of anthropogenic mercury based on water column measurements. *Nature*, *512*(7512), 65–68. https://doi.org/10.1038/nature13563

Lemelle, L., Bartolini, A., Simionovici, A., Tucoulou, R., De Nolf, W., Bassinot, F., & de Garidel-Thoron, T. (2020). Nanoscale trace metal imprinting of biocalcification of planktic foraminifers by Toba's super-eruption. *Scientific Reports*, *10*(1), 10974. https://doi.org/10.1038/s41598-020-67481-w

Littler, K., Röhl, U., Westerhold, T., & Zachos, J. C. (2014). A high-resolution benthic stable isotope record for the South Atlantic: Implications for orbital-scale changes in late Paleocene–early Eocene climate and carbon cycling. *Earth and Planetary Science Letters*, *401*, 18–30. https://doi.org/10.1016/j.epsl.2014.05.054

Liu, M., Zhang, Q., Maavara, T., Liu, S., Wang, X., & Raymond, P. A. (2021). Rivers as the largest source of mercury to coastal oceans worldwide. *Nature Geoscience*, *14*(9), 672–677. https://doi.org/10.1038/s41561-021-00793-2

Lourens, L. J., Sluijs, A., Kroon, D., Zachos, J. C., Thomas, E., Röhl, U., et al. (2005). Astronomical pacing of late Palaeocene to early Eocene global warming events. *Nature*, *435*(7045), 1083–1087. https://doi.org/10.1038/nature03814

Luciani, V. (1989). Stratigrafia sequenziale del Terziario nella catena del Monte Baldo (Provincie di Verona e Trento). *Memorie di Scienze Geologiche*, *41*, 263–351.

Luciani, V., D'Onofrio, R., Dickens, G. R., & Wade, B. S. (2017a). Did photosymbiont bleaching lead to the demise of planktic foraminifer *Morozovella* at the Early Eocene Climatic Optimum? *Paleoceanography*, *32*(11), 1115–1136. https://doi.org/10.1002/2017PA003138

Luciani, V., D'Onofrio, R., Dickens, J. R., & Wade, B. S. (2017b). Planktic foraminiferal response to early Eocene carbon cycle perturbations in the southeast Atlantic Ocean (ODP Site 1263). *Global and Planetary Change*, *158*, 119–133. https://doi.org/10.1016/j.gloplacha.2017.09.007

Luciani, V., D'Onofrio, R., Filippi, G., & Moretti, S. (2020). Which was the habitat of early Eocene foraminifer *Chiloguembelina*? Stabel isotope paleobiology from the Atlantic Ocean and implication for paleoceanographic reconstructions. *Global and Planetary Change*, *191*, 103216. https://doi.org/10.1016/j.gloplacha.2020.103216

Luciani, V., Giusberti, L., Agnini, C., Backman, J., Fornaciari, E., & Rio, D. (2007). The Paleocene–Eocene Thermal Maximum as recorded by Tethyan planktonic foraminifera in the Forada section (northern Italy). *Marine Micropaleontology*, *64*(3), 189–214. https://doi.org/10.1016/j.marmicro.2007.05.001

Luterbacher, H. P., & Premoli, S. I. (1964). Biostratigrafia del limite Cretaceo-Terziario nell'Appennino centrale. *Rivista Italiana di Paleontologia e Stratigrafia*, *70*, 67–128.

Mancini, A. M., Grelaud, M., Ziveri, P., Nallino, E., & Lozar, F. (2021). Calcareous nannofossil size and abundance response to the Messinian Salinity Crisis onset and paleoenvironmental dynamics. *Paleoceanography and Paleoclimatology*, *36*(9), e2020PA004155. https://doi.org/10.1029/2020PA004155

Mason, R. P., & Sheu, G. R. (2002). Role of the ocean in the global mercury cycle. *Global Biogeochemical Cycles*, *16*(4), 40-1–40-14. https://doi.org/10.1029/2001GB001440

Murray, J. W. (1991). *Ecology and palaeoecology of benthic foraminifera* (p. 397). Longman.

Nguyen, T. M. P., Petrizzo, M.-R., & Speijer, R. P. (2009). Experimental dissolution of a fossil foraminiferal assemblage (Paleocene–Eocene Thermal Maximum, Dababiya, Egypt): Implications for paleoenvironmental reconstructions. *Marine Micropaleontology*, *73*(3–4), 241–258. https://doi.org/10.1016/j.marmicro.2009.10.005

Nguyen, T. M. P., Petrizzo, M.-R., Stassen, P., & Speijer, R. P. (2011). Dissolution susceptibility of Paleocene–Eocene planktic foraminifera: Implications for palaeoceanographic reconstructions. *Marine Micropaleontology*, *81*(1–2), 1–21. https://doi.org/10.1016/j.marmicro.2011.07.001

Nigam, R., Linshy, V. N., Kurtarkar, S. R., & Saraswat, R. (2009). Effects of sudden stress due to heavy metal mercury on benthic foraminifer *Rosalina leei*: Laboratory culture experiment. *Marine Pollution Bulletin*, *59*(8–12), 362–368. https://doi.org/10.1016/j.marpolbul.2009.08.014

Nigam, R., Saraswat, R., & Panchang, R. (2006). Application of foraminifers in ecotoxicology: Retrospect, perspect and prospect. *Environment International*, *32*(2), 273–283. https://doi.org/10.1016/j.envint.2005.08.024

O'Connor, M., Piehler, M. F., Leech, D. M., Anton, A., & Bruno, J. F. (2009). Warming and resource availability shift food web structure and metabolism. *PLoS Biology*, *7*(8), e1000178. https://doi.org/10.1371/journal.pbio.1000178

Okada, H., & Bukry, D. (1980). Supplementary modification and introduction of code numbers to the low latitude coccolith biostratigraphy zonation (Bukry, 1973, 1975). *Marine Micropaleontology*, *51*, 321–325. https://doi.org/10.1016/0377-8398(80)90016-X

Ortiz, J. D., Mix, A. C., & Collier, R. W. (1995). Environmental control of living symbiotic and asymbiotic foraminifera of the California Current. *Paleoceanography*, *10*(6), 987–1009. https://doi.org/10.1029/95pa02088

Oschlies, A., Brandt, P., Stramma, L., & Schmidtko, S. (2018). Drivers and mechanisms of ocean deoxygenation. *Nature Geoscience*, *11*(7), 467–473. https://doi.org/10.1038/s41561-018-0152-2

Papazzoni, C. A., Giusberti, L., & Trevisani, E. (2014). The Spilecco site. In C. A. Papazzoni, L. Giusberti, G. Carnevale, G. Roghi, D. Bassi, & R. Zorzin (Eds.), *The Bolca Fossil-Lagerstätten: A window into the Eocene World* (pp. 105–110). Rendiconti della Società Paleontologica.

Pearson, P. N., Olsson, R. K., Hemblen, C., Huber, B. T., & Berggren, W. A. (Eds.) (2006). *Atlas of Eocene Planktonic Foraminifera, Cushman Special Publication, Department of Geology East Carolina Univ, Greenville* (p. 513).

Percival, L. M. E., Witt, M. L. I., Mather, T. A., Hermoso, M., Jenkyns, H. C., Hesselbo, S. P., et al. (2015). Globally enhanced mercury deposition during the end-Pliensbachian extinction and Toarcian OAE: A link to the Karoo-Ferrar large Igneous Province. *Earth and Planetary Science Letters*, *428*, 267–280. https://doi.org/10.1016/j.epsl.2015.06.064

Pörtner, H.-O., Roberts, D. C., Tignor, M., Poloczanska, E. S., Mintenbeck, K., Alegría, A., et al. (Eds.) (2022). *IPCC 2022: Climate change 2022: Impacts, adaptation and vulnerability. Contribution of working group II to the sixth assessment report of the intergovernmental panel on climate change* (p. 3056). Cambridge University Press. Cambridge University Press. https://doi.org/10.1017/9781009325844

Rillo, M. C., Miller, C. G., Kucera, M., & Ezard, T. H. G. (2020). Intraspecific size variation in planktonic foraminifera cannot be consistently predicted by the environment. *Ecology and Evolution*, *10*(20), 11579–11590. https://doi.org/10.1002/ece3.6792

Sanei, H., Grasby, S. E., & Beauchamp, B. (2012). Latest Permian mercury anomalies. *Geology*, *40*(1), 63–66. https://doi.org/10.1130/G32596.1

Saraswat, R., Kurtarkar, S. R., Mazumder, A., & Nigam, R. (2004). Foraminifers as indicators of marine pollution: A culture experiment with *Rosalina leei*. *Marine Pollution Bulletin*, *48*(1–2), 91–96. https://doi.org/10.1016/s0025-326x(03)00330-8

Schlanger, S., & Jenkyns, H. (1976). Cretaceous oceanic anoxic events: Causes and consequences. *Geologie en Mijnbouw*, *55*(3–4), 179–184.

Schmidt, D. N., Lazarus, D., Young, J. R., & Kucera, M. (2006). Biogeography and evolution of body size in marine plankton. *Earth-Science Reviews*, *78*(3–4), 239–266. https://doi.org/10.1016/j.earscirev.2006.05.004

Schmidt, D. N., Renaud, S., Bollmann, J., Schiebel, R., & Thierstein, H. R. (2004). Size distribution of Holocene planktic foraminifer assemblages: Biogeography, ecology and adaptation. *Marine Micropaleontology*, *50*(3–4), 319–338. https://doi.org/10.1016/S0377-8398(03)00098-7

Schrag, D. P., DePaolo, D. J., & Richter, F. M. (1995). Reconstructing past sea surface temperatures: Correcting for diagenesis of bulk marine carbonate. *Geochimica et Cosmochimica Acta*, *59*(11), 2265–2278. https://doi.org/10.1016/0016-7037(95)00105-9

Sluijs, A., Schouten, S., Donders, T. H., Schoon, P. L., Röhl, U., Reichart, G.-J., et al. (2009). Warm and wet conditions in the Arctic region during Eocene Thermal Maximum 2. *Nature Geoscience*, *2*(11), 1–4. https://doi.org/10.1038/ngeo668

Spero, H. J., & DeNiro, M. J. (1987). The influence of photosynthesis on the $\delta^{18}O$ and $\delta^{13}C$ values of planktonic foraminiferal shell calcite. *Symbiosis*, *4*, 213–228.

Stap, L., Lourens, L. J., Thomas, E., Sluijs, A., Bohaty, S., & Zachos, J. C. (2010a). High-resolution deep-sea carbon and oxygen isotope records of Eocene Thermal Maximum 2 and H2. *Geology*, *38*(7), 607–610. https://doi.org/10.1130/G30777.1

Stap, L., Lourens, L. J., van Dijk, A., Schouten, S., & Thomas, E. (2010b). Coherent pattern and timing of the carbon isotope excursion and warming during Eocene Thermal Maximum 2 as recorded in planktic and benthic foraminifera. *Geochemistry, Geophysics, Geosystems*, *11*, Q11011. https://doi.org/10.1029/2010GC003097

Stap, L., Sluijs, A., Thomas, E., & Lourens, L. J. (2009). Patterns and magnitude of deep sea carbonate dissolution during Eocene Thermal Maximum 2 and H2, Walvis Ridge, Southeastern Atlantic Ocean. *Paleoceanography*, *24*(1), PA1211. https://doi.org/10.1029/2008PA001655

Sunderland, E. M., Krabbenhoft, D. P., Moreau, J. W., Strode, S. A., & Landing, W. M. (2009). Mercury sources, distribution, and bioavailability in the North Pacific Ocean: Insights from data and models. *Global Biogeochemical Cycles*, *23*(3), GB2010. https://doi.org/10.1029/2008GB003425

ThemJagoe, T. R. C. H., Caruthers, H. A., Gill, B. C., Grasby, S. E., Gröcke, D. R., Yin, D., & Owens, J. D. (2019). Terrestrial sources as the primary delivery mechanism of mercury to the oceans across the Toarcian Oceanic Anoxic Event (Early Jurassic). *Earth and Planetary Science Letters*, *507*, 62–72. https://doi.org/10.1016/j.epsl.2018.11.029

Thomas, E., Zachos, J. C., & Bralower, T. J. (2000). Deep-sea environments on a warm Earth: Latest Paleocene–early Eocene. In B. Huber, K. MacLeod, & S. Wing (Eds.), *Warm climates in earth history* (pp. 132–160). Cambridge Univ. Press.

Tjalsma, R. C., & Lohmann, G. P. (1983). Paleocene-Eocene bathyal and abyssal benthic foraminifera from the Atlantic Ocean. *Micropaleontology*, *4*, 76–90.

Todd, C. L., Schmidt, D. N., Robinson, M. M., & De Schepper, S. (2020). Planktic foraminiferal test size and weight response to the late Pliocene environment. *Paleoceanography and Paleoclimatology*, *35*(1), e2019PA003738. https://doi.org/10.1029/2019PA003738

Tremolada, F., De Bernardi, B., & Erba, E. (2008). Size variations of the calcareous nannofossil taxon Discoaster multiradiatus (Incertae sedis) across the Paleocene–Eocene thermal maximum in ocean drilling program holes 690B and 1209B. *Marine Micropaleontology*, *67*(3–4), 239–254. https://doi.org/10.1016/j.marmicro.2008.01.010

Van Morkhoven, F. P. C. M., Berggren, W. A., & Edwards, A. S. (1986). Cenozoic cosmopolitan deep-water benthic foraminifera. *Bulletin des Centres de Recherches Exploration-Production Elf-Aquitaine - Memoire*, *11*, 1–421.

Wade, B. S., Pearson, P. N., Berggren, W. A., & Pälike, H. (2011). Review and revision of Cenozoic tropical planktonic foraminiferal biostratigraphy and calibration to the geomagnetic polarity and astronomical time scale. *Earth-Science Reviews*, *104*(1–3), 111–142. https://doi.org/10.1016/j.earscirev.2010.09.003

Wells, J. D., & Mullens, T. E. (1973). Gold-bearing arsenian pyrite determined by microprobe analyses, Cortez and Carlin mines, Nevada. *Economic Geology*, *68*(2), 187–201. https://doi.org/10.2113/gsecongeo.68.2.187

Westerhold, T., Marwan, N., Drury, A. J., Liebrand, D., Agnini, C., Anagnostou, E., et al. (2020). An astronomically dated record of Earth's climate and its predictability over the last 66 million years. *Science*, *369*(6509), 1383–1387. https://doi.org/10.1126/science.aba6853

Westerhold, T., Röhl, U., Donner, B., & Zachos, J. C. (2018). Global Extent of early Eocene Hyperthermal events: A New Pacific Benthic Foraminiferal Isotope Record From Shatsky rise (ODP Site 1209). *Paleoceanography and Paleoclimatology*, *33*(6), 626–642. https://doi.org/10.1029/2017PA003306

Zachos, J. C., Dickens, G. R., & Zeebe, R. E. (2008). An early Cenozoic perspective on greenhouse warming and carbon-cycle dynamics. *Nature*, *451*(7176), 279–283. https://doi.org/10.1038/nature06588

Zachos, J. C., McCarren, H. K., Murphy, B., Röhl, U., & Westerhold, T. (2010). Tempo and scale of late Paleocene and early Eocene carbon isotope cycles: Implications for the origin of hyperthermals. *Earth and Planetary Science Letters*, *299*(1–2), 242–249. https://doi.org/10.1016/j.epsl.2010.09.004

Zachos, J. C., Röhl, U., Schellenberg, S. A., Sluijs, A., Hodell, D. A., Kelly, D. C., et al. (2005). Rapid acidification of the ocean during thePaleocene–Eocene Thermal Maximum. *Science*, *308*(5728), 1611–1615. https://doi.org/10.1126/science.1109004

Zeebe, R. E., Zachos, J. C., & Dickens, G. R. (2009). Carbon dioxide forcing alone insufficient to explain Palaeocene–Eocene Thermal Maximum warming. *Nature Geoscience*, *2*(8), 576–580. https://doi.org/10.1038/ngeo578

Zintwana, M. P., Cawthorn, R. G., Ashwal, L. D., Roelofse, F., & Cronwright, H. (2012). Mercury in the Bushveld complex, South Africa, and the Skaergaard intrusion, Greenland. *Chemical Geology*, *320*, 147–155. https://doi.org/10.1016/j.chemgeo.2012.06.001

References From the Supporting Information

Grasby, S. E., Sanei, H., Beauchamp, B., & Chen, Z. H. (2013). Mercury deposition through the Permo-Triassic biotic crisis. *Chemical Geology*, *351*, 209–216. https://doi.org/10.1016/j.chemgeo.2013.05.022